Opblazen lantaarnpaal

Origineel bij ir. Houtacker.

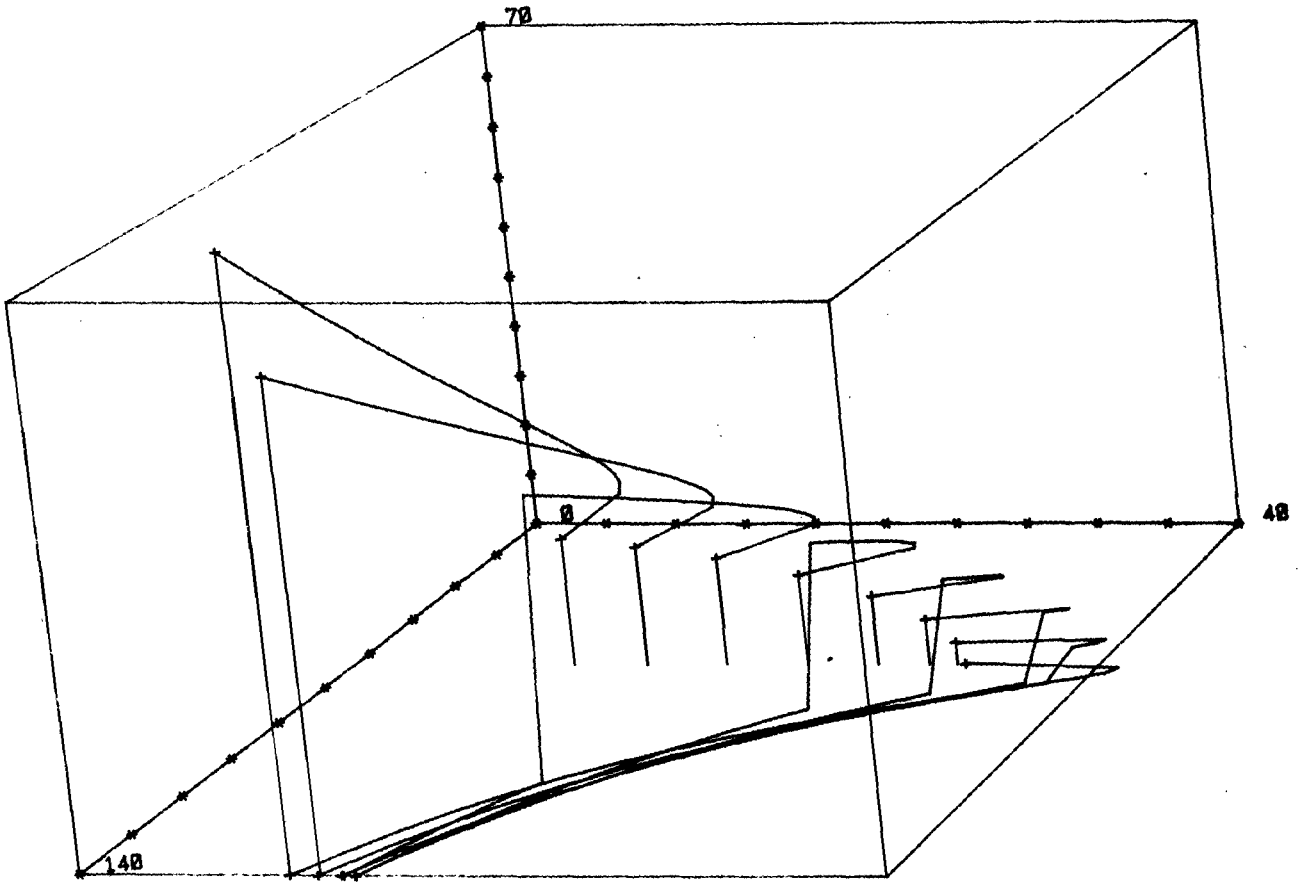

OPBLAZEN LANTAARNPAAL

auteur: J. Vosmer.

WPT-rapport nr. 0537.

april '82

Opblazen Lantaarnpaal (I-1 stage Jan Vosmer)

Gedachtenstreepjes van prof. J.A.G. Kals:

Bij het uitvoeren van berekening t.b.v. de buisexpansie komt het nuttig de volgende invloeden op de een of andere wijze mede te verantwoorden:

- koudversteviging v/h buismateriaal
- conciciteit i.v.m. correctie op axiale komponent v/d drukkracht
- correctie op de kracht i.v.m. hydraulische druk op de kopvlakken v/h gereedschap
- spanningsverloop over de wanddikte i.v.m. kiezen van buiten of binnenvlak als referentie voor d/d proces regeling
- gevoeligheidsanalyse van fluctuaties in een aantal procesgrootheden t.b.v. controle op procesverloop
- globale grenzen v/h regelbereik tussen enerzijds de grens vervormingskromme en anderzijds gevarengebied voor globale en plaatselijke knik. E.e.a. naar behoefte

Overige aspecten welke voorlopig van minder belang lijken en mogelijk v/d uitvoeringswijze van de machine afhangen:

- wrijving
- anisotropie.

Het uiteindelijke doel is het vervaardigen van in licht konisch verlopende lantaarnpaal uit hetzelfde materiaal als waaruit ze nu vervaardigd worden.

Gebruikte symbolen

d	momentane binnendiameter buis resp. bol	[mm]
t	momentane wanddikte	[mm]
t_o	wanddikte bij begin vervorming	[mm]
d_o	binnendiameter " " "	[mm]
L	momentane buislengte	[mm]
l_o	buislengte bij begin vervorming	[mm]
d_1	gewenste eind-binnendiameter	[mm]
d_k	kritische diameter of overgangsdiameter	[mm]
r	~~binnen~~ straal	[mm]
z	axiale coördinaat-aanduiding	[mm]
φ	tangentiale hoek (in vlak $\perp$ z-richting)	[-]
θ	hoek tussen r-richting en φ-vlak	[-]
θ_k	kritische hoek θ behorend bij overgangsdiamter d_k	[-]
C	constante in verstevigingswet van Nadai	[N/mm^2]
n	verstevigingsexponent	[-]
A	oppervlak	[mm^2]
f	wrijvingscoefficient	[-]
λ	belastingparameter	[-]
F_{ax}	axiale kracht	[N]
F_{pers}	perskracht	[N]
$\sigma_z, \sigma_\varphi, \sigma_r, \sigma_\theta$	spanningen in de hoofdrichtingen	[N/mm^2]
$\sigma_{zr}, \sigma_{z\varphi}, \sigma_{r\varphi}$	schuifspanningen	[N/mm^2]

Gedachte achter het proces is het aanbrengen van 'n axiaalkracht, waardoor 'n axiale drukspanning ontstaat en middels de inwendige druk een tangentiele trekspanning veroorzaken, zodat 'n spanningstoestand ontstaat die het materiaal accepteert.

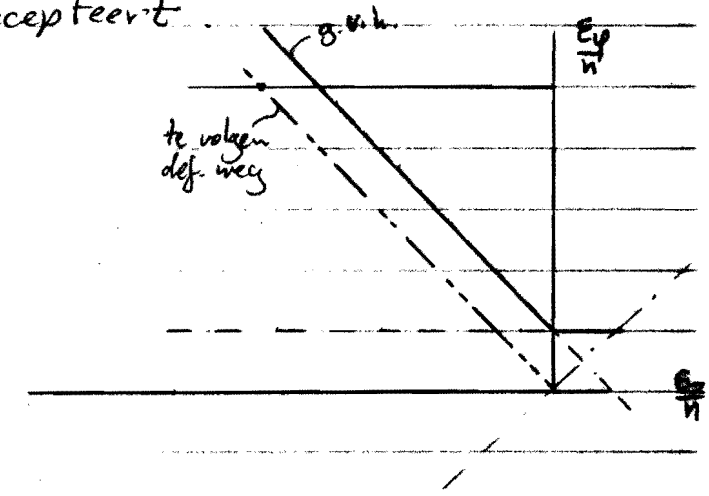

Eenvoudig opblazen van een cilinder:

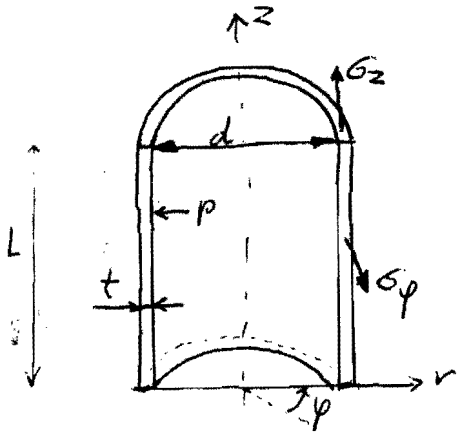

Onderstel $t/d \ll 1$ en t constant

$F_{ax} = \sigma_z \cdot \pi\, d \cdot t$

$p \cdot d \cdot L = 2 \cdot \sigma_\varphi \cdot L \cdot t \rightarrow p = \frac{2 \cdot \sigma_\varphi \cdot t}{d}$

Volume-invariantie: $L \cdot d \cdot t = L_o \cdot d_o \cdot t_o$

met $t = t_o$: $L \cdot d = L_o \cdot d_o$

$\varepsilon_z = \ln \frac{L}{L_o} = -\varepsilon_\varphi = -\ln \frac{d}{d_o}$

$\sigma_r = 0$; $\sigma_z = -\sigma_\varphi$; $\bar{\sigma} = \sqrt{3} \cdot \sigma_\varphi$; $\frac{\bar{\varepsilon}}{\bar{\sigma}} = C^{\frac{-1}{n}} \cdot \bar{\sigma}^{\frac{1-n}{n}}$

Levy-von Mises: $\varepsilon_z = -\frac{3}{2} \frac{\bar{\varepsilon}}{\bar{\sigma}} \sigma_\varphi$

$\varepsilon_\varphi = \frac{3}{2} \frac{\bar{\varepsilon}}{\bar{\sigma}} \sigma_\varphi$

dus $\ln \frac{d}{d_o} = \frac{3}{2} \cdot C^{\frac{-1}{n}} \cdot \bar{\sigma}^{\frac{1-n}{2n}} \cdot \sigma_\varphi$ * $\rightarrow \ln \frac{d}{d_o} = \frac{3}{2} \cdot C^{\frac{-1}{n}} \cdot 3^{\frac{1-n}{2n}} \cdot \sigma_\varphi^{\frac{1}{n}}$

Hieruit volgt $\sigma_\varphi = \frac{2^n \cdot C}{3^{\frac{1+n}{2}}} \cdot \left(\ln \frac{d}{d_0}\right)^n$

d.i. $F = -\pi \cdot d \cdot t \cdot \frac{2^n \cdot C}{3^{\frac{1+n}{2}}} \cdot \left(\ln \frac{d}{d_0}\right)^n$

$$p = \frac{2t}{d} \cdot \frac{2^n \cdot C}{3^{\frac{1+n}{2}}} \left(\ln \frac{d}{d_0}\right)^n$$

$$\boxed{\frac{F}{p} = -\frac{\pi}{2} \cdot d^2}$$

Aan de laatste vergelijking dient het hele proces te voldoen van begin tot het eind.

Nettere berekening met σ_r

Onderskel wanddikte blijft constant, dus $\varepsilon_z = -\varepsilon_\varphi$

Globaal e.w. $F = \int_{A_r} \sigma_z \, dA_r = 2\pi \int_{r=\frac{d}{2}}^{r=\frac{d}{2}+t} \sigma_z \cdot r \, dr$

$$\int_{r=-\frac{d}{2}}^{\frac{d}{2}} dr \int_{z=0}^{L} p \, dz = \int_{A_L} \sigma_\varphi \, dA_L = 2 \int_{z=0}^{L} dz \int_{r=\frac{d}{2}}^{\frac{d}{2}+t} \sigma_\varphi \, dr$$

Volume-invariantie: $\frac{\pi}{4}\left((d+2t)^2 - d^2\right) \cdot L = \frac{\pi}{4}\left((d_0+2t_0)^2 - d_0^2\right) \cdot L_0$

met $t = t_0$: $L(d+t_0) = L_0(d_0+t_0)$

$\varepsilon_z = \ln \frac{L}{L_0}$

$\varepsilon_\varphi = \ln \frac{d+t_0}{d_0+t_0}$

$\varepsilon_r = 0$

L.v.M.: $\varepsilon_z = \frac{\bar{\varepsilon}}{\bar{\sigma}}\left(\sigma_z - \frac{\sigma_r + \sigma_\varphi}{2}\right)$

$\varepsilon_\varphi = \frac{\bar{\varepsilon}}{\bar{\sigma}}\left(\sigma_\varphi - \frac{\sigma_r + \sigma_z}{2}\right)$

$$\varepsilon_r = \frac{\bar{\varepsilon}}{\bar{\sigma}}\left(\sigma_r - \frac{\sigma_z+\sigma_\varphi}{2}\right)$$

Substitutie van $\varepsilon_z = -\varepsilon_\varphi$ levert $\sigma_r = \frac{\sigma_z+\sigma_\varphi}{2}$

$$2\bar{\sigma}^2 = (\sigma_r-\sigma_z)^2 + (\sigma_\varphi-\sigma_r)^2 + (\sigma_z-\sigma_\varphi)^2 = \frac{3}{2}\left(\sigma_\varphi^2+\sigma_z^2-2\sigma_\varphi\cdot\sigma_z\right)$$

$$\text{dus}\quad \bar{\sigma} = \sqrt{\tfrac{4}{3}\left(\sigma_\varphi^2+\sigma_z^2-2\sigma_\varphi\sigma_z\right)}$$

Lokaal evenwicht : $\sigma_{zr} = \sigma_{z\varphi} = \sigma_{r\varphi} = 0$

$$\begin{cases} \frac{\partial\sigma_r}{\partial r} + \frac{\sigma_r-\sigma_\varphi}{r} = 0 \\ \frac{1}{r}\frac{\partial\sigma_\varphi}{\partial\varphi} = 0 \quad\rightarrow\quad \sigma_\varphi \neq \sigma_\varphi(\varphi) \\ \frac{\partial\sigma_z}{\partial z} = 0 \quad\rightarrow\quad \sigma_z \neq \sigma_z(z) \end{cases}$$

$\sigma_\varphi = r\frac{\partial\sigma_r}{\partial r} + \sigma_r$; Oplossing $\sigma_r\left(r=\frac{d}{2}\right) = -p$

$\sigma_r\left(r=\frac{d}{2}+t_0\right) = 0$

en σ_r lineair verdeeld over wand

d.i. $\sigma_r = -p\left(1+\frac{d-2r}{2t_0}\right)$

d.i. $\sigma_\varphi = -p\left(1+\frac{d-4r}{2t_0}\right)$

Er geldt dat $\sigma_r = \frac{\sigma_\varphi+\sigma_z}{2}$ dus $\sigma_z = 2\sigma_r-\sigma_\varphi = -p\left(1+\frac{d}{2t_0}\right)$

Opmerking : $\sigma_\varphi > |\sigma_z|$

$\bar{\sigma} = \sqrt{\tfrac{4}{3}\left(\sigma_\varphi^2+\sigma_z^2-2\sigma_\varphi\sigma_z\right)} = \sqrt{3}\cdot\frac{p\cdot r}{t_0}$; vloeien treedt dus het eerst op aan de buitenkant van de cilinder

$$F = 2\pi\int_{r=\frac{d}{2}}^{\frac{d}{2}+t_0}\sigma_z\, r\,dr = 2\pi\int_{\frac{d}{2}}^{\frac{d}{2}+t_0} -p\left(1+\frac{d}{2t_0}\right) r\,dr = -\frac{\pi}{2}\cdot p\,(d+2t_0)(d+t_0$$

Hieruit volgt : $\boxed{\frac{F}{p} = -\frac{\pi}{2}\left(d^2 + 3\cdot t_o \cdot d + 2t_o^2\right)}$ (vgl. relatie blz.

De spanningen voldoen ook aan de tweede vgl. Vh globaal e.w. !

Er doet zich in maximale druk voor tijdens het proces ; Bij welke diameter vindt die druk plaats

$p = \frac{\bar{\sigma}\cdot t_o}{\sqrt{3}\cdot r}$ p_{max} treedt op voor $r = \frac{d}{2}$

dus $p = \frac{2\bar{\sigma}\, t_o}{\sqrt{3}\cdot d}$ substitutie van Nadai met $\bar{\varepsilon}^2 = \frac{4}{3}\varepsilon_1^2$

levert dat $p \sim \frac{1}{d}\left(\ln\frac{d+t_o}{d_o+t_o}\right)^n$

$\frac{\partial p}{\partial d} = \frac{-1}{d^2}\left(\ln\frac{d+t_o}{d_o+t_o}\right)^n + \frac{1}{d}\left(\ln\frac{d+t_o}{d_o+t_o}\right)^{n-1}\cdot\frac{1}{d+t_o} = 0$

Neem voor de eenvoud aan dat $t_o \ll d$, d.i. de enige interessante waarde waarvoor $\frac{\partial p}{\partial d} = 0$:

$\boxed{d_k = d_o \exp n}$

Intermezzo :

Volume-invariantie conische pijp

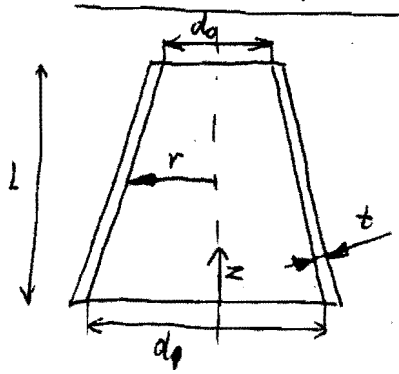

$r = \frac{1}{2}d_1 - \frac{z}{L}\left(\frac{d_1-d_o}{2}\right)$; $A = \pi\cdot d_o\cdot L + \frac{\pi}{2}(d_1-d_o)\cdot L$ indien flauw conisch !

Begininhoud $= \pi\cdot d_o\cdot L_o\cdot t_o$

~~Materiaal~~ Eind-inhoud $= \frac{\pi}{2}L(d_1+d_o)\cdot t$

Indien $t = t_o$ dan geldt $L_o = L\cdot\frac{d_1+d_o}{2\cdot d_o}$

Voor $d_1 = 140$ mm , $d_o = 60$ mm geldt $L_o = \frac{5}{3}\cdot L$, d.w.z. 40% rea

Indien F' alleen opgevangen wordt door de buis, wordt de vlaktedruk te hoog. F' wordt ook opgevangen door de 'matrijs', indien de wrijving tussen buis en matrijs voldoe groot is.

$$A_w = A_{wrijving} = \frac{\pi}{2} \cdot L(d+d_0) = \frac{\pi}{2} \cdot \frac{d_0}{d} \cdot l_0 (d+d_0) \qquad (t=t_0)$$

Coulombse wrijving: $F_w = p \cdot A_w \cdot f$; $F_{wx} = f \cdot p \cdot A_w \cdot \cos\alpha \approx f \cdot p \cdot \frac{\pi}{2} \cdot f \cdot \frac{d_0}{d} \cdot l_0 (d+d_0) \cdot p$

$$F' = F + \frac{\pi}{4} \cdot p (d^2 - d_0^2) = \left(\frac{3}{4} d^2 - \frac{1}{4} d_0^2 + \frac{3}{2} t_0 \cdot d + t_0^2 \right) \cdot \pi \cdot p$$

$$h_1 = \frac{F_{wx}}{\pi \cdot p} = \frac{1}{2} \cdot f \cdot d_0 \cdot l_0 \left(1 + \frac{d_0}{d} \right)$$

$$h_2 = \frac{F'}{\pi \cdot p} = \frac{3}{4} d^2 - \frac{1}{4} d_0^2 + \frac{3}{2} t_0 \cdot d + t_0^2$$

$$\frac{l_0}{d_0} \approx \frac{6700}{60} \approx 110 \,;\; f \approx 0.1 \Rightarrow \quad f \cdot l_0 \approx 11 \cdot d_0$$

Wortels van h_2: $d_{1,2} = -t_0 \pm \frac{1}{3}\sqrt{3}\sqrt{d_0^2 - t_0^2}$

$h_2(d=d_0) = \frac{1}{2} d_0^2 + \frac{3}{2} t_0 d_0 + t_0^2$

$h_2(d=2d_0) = 2\frac{3}{4} d_0^2 + 3 t_0 d_0 + t_0^2$

$h_2(d=3d_0) = 6\frac{1}{2} d_0^2 + \frac{9}{2} t_0 d_0 + t_0^2$

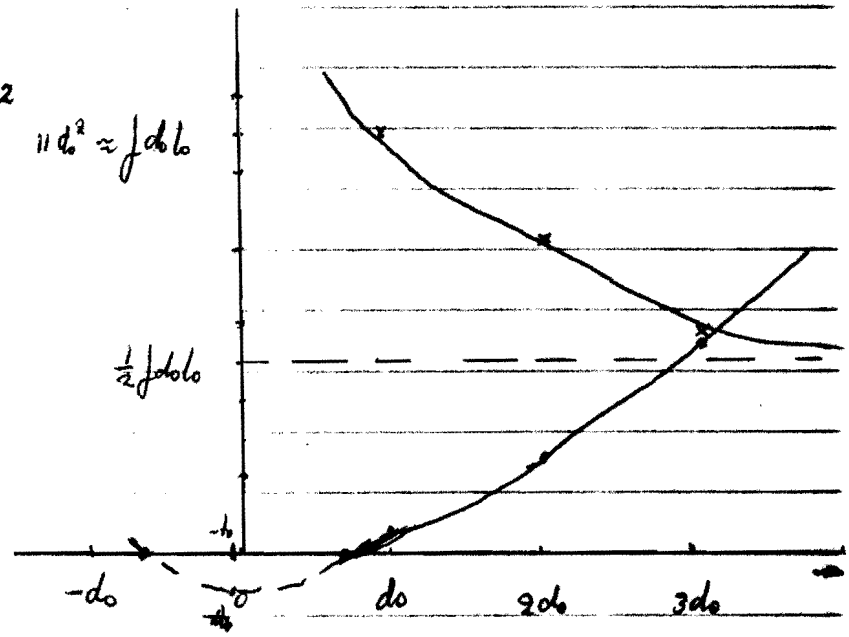

Schaalmodel

geometrisch gelijkvormig : $\frac{l}{l_m} = \frac{d}{d_m} = \frac{t}{t_m} = c$

m = model ; e = eindsituatie ; o = uitgangssituatie

Onderstel $t_o = t_e$ dus $t_{mo} = t_{me}$

$$p = 2^{n+1} \cdot 3^{-\frac{n+1}{2}} \cdot \frac{C \cdot t_o}{d} \left[\ln \frac{d+t_o}{d_o+t_o} \right]^n \qquad \frac{t_o}{d} = \frac{t_{mo}}{d_m} \text{ en}$$

$\frac{d+t_o}{d_o+t_o} = \frac{d_m+t_{mo}}{d_{mo}+t_{mo}}$, dus in het schaalmodel moet eenzelfde druk gehanteerd worden als in het aanvankelijke model.

$F = -\frac{\pi}{2}(d^2 + 3t_o d + 2t_o^2) \cdot p$ wordt in het schaalmodel

kwadratisch kleiner met c

Conclusie : De verwachting, dat met een schaalmodel een lagere druk nodig zou zijn voor het proces (veiligheid), komt niet uit. Het heeft dan ook weinig zin om met 'n schaalmodel te werken.

Wrijving wand matrijs en aanliggende buis

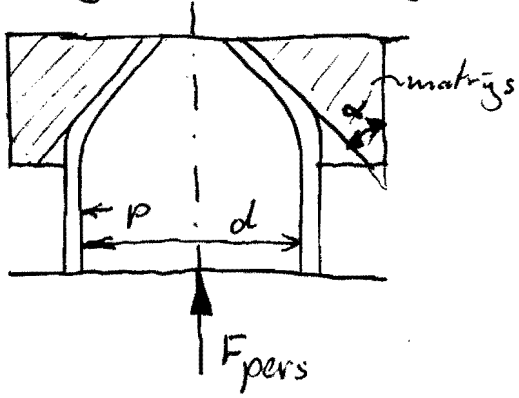

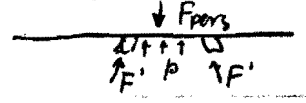

$P_{pers} = F' + p \cdot \frac{\pi}{4} d_o^2$

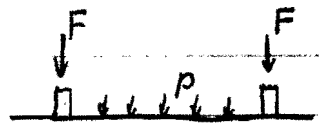

$F_{pers} = F + p \cdot \frac{\pi}{4} d^2$

$h_1 > h_2$, d.w.z. F_{wex} is voldoende groot ($bt \pm 3 d_0$) om de axiale kracht t.g.v. conicaiteit en druk door te leiden naar de matrys.

$$\frac{F_{pers}}{p} = -\pi \left[\frac{3}{4} d^2 + \frac{3}{2} t_0 \, d + t_0^2 \right]$$

Berekening met variabele rekweg.

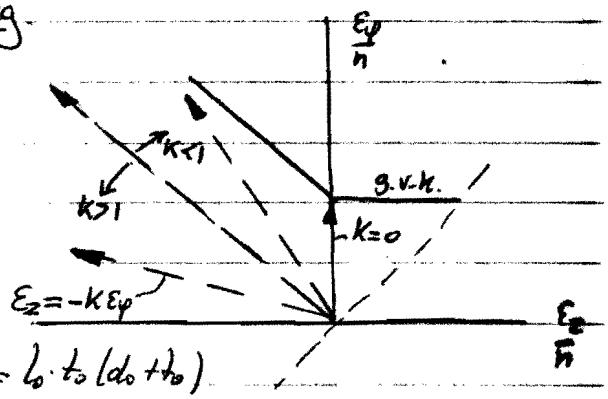

$\varepsilon_z = -k \cdot \varepsilon_\varphi$
$\varepsilon_r = (k-1) \cdot \varepsilon_\varphi$
$\varepsilon_z : \varepsilon_\varphi : \varepsilon_r = -k : 1 : k-1$

Volume-invariantie. $L \cdot t (d+t) = l_0 \cdot t_0 (d_0 + t_0)$

L.v.M.:
$$\varepsilon_z = \frac{\varepsilon}{\sigma}\left(\sigma_z - \frac{\sigma_r + \sigma_\varphi}{2}\right)$$
$$\varepsilon_\varphi = \frac{\varepsilon}{\sigma}\left(\sigma_\varphi - \frac{\sigma_r + \sigma_z}{2}\right)$$
$$\varepsilon_r = \frac{\varepsilon}{\sigma}\left(\sigma_r - \frac{\sigma_\varphi + \sigma_z}{2}\right)$$

Met $\varepsilon_z = -k \cdot \varepsilon_\varphi$ levert dit: $\sigma_z - \frac{\sigma_r + \sigma_\varphi}{2} = -k \cdot \left(\sigma_\varphi - \frac{\sigma_z + \sigma_r}{2}\right)$

$$\Rightarrow \sigma_\varphi = \frac{k+1}{2k-1}\sigma_r - \frac{2-k}{2k-1} \cdot \sigma_z$$

$$\varepsilon_z = \ln \frac{L}{l_0}$$
$$\varepsilon_\varphi = \ln \frac{d+t}{d_0+t_0}$$
$$\varepsilon_r = \ln \frac{t}{t_0}$$

Lokaal e.w.
$$\frac{\partial \sigma_r}{\partial r} + \frac{\sigma_r - \sigma_\varphi}{r} = 0$$
$$\frac{1}{r}\frac{\partial \sigma_\varphi}{\partial \varphi} = 0$$
$$\frac{\partial \sigma_z}{\partial z} = 0$$

(A) Onderstel σ_z is constant over de wanddikte: $\sigma_z = S_z$
d.i. $\sigma_r = \frac{2-k}{k+1} \cdot S_z + \frac{2k-1}{k+1} \cdot \sigma_\varphi$
Substitutie in lokaal e.w. levert op: $\sigma_\varphi = S_z + r^{\frac{2-k}{2k-1}} + C_2$

d.i. $\sigma_r = \frac{2-k}{k+1}\cdot S_z + \frac{2k-1}{k+1}\left[S_z + r^{\frac{2-k}{2k-1}} + C_2\right]$

$\sigma_r\left(r=\frac{d}{2}\right) = -p \;\rightarrow\; C_2 = -\frac{k+1}{2k-1}(p+S_z) - \left(\frac{d}{2}\right)^{\frac{2-k}{2k-1}}$

spanningen: $\sigma_z = S_z$

$\sigma_\varphi = S_z + r^{\frac{2-k}{2k-1}} - \frac{k+1}{2k-1}(p+S_z) - \left(\frac{d}{2}\right)^{\frac{2-k}{2k-1}}$

$\sigma_r = -p + \frac{2k-1}{k+1}\left[r^{\frac{2-k}{2k-1}} - \left(\frac{d}{2}\right)^{\frac{2-k}{2k-1}}\right]$

Noot: aan de rvw. $\sigma_r\left(r=\frac{d}{2}+t\right)=0$ wordt niet voldaan.

$$F = 2\pi \int_{r=\frac{d}{2}}^{\frac{d}{2}+t} S_z\, r\, dr = \pi\cdot S_z\cdot t(d+t)$$

$$p\cdot d\cdot l = 2\int_{z=0}^{l} dz \int_{r=\frac{d}{2}}^{\frac{d}{2}+t} \sigma_\varphi\, dr \;\Rightarrow$$

$$p = \frac{2}{d}\left\{ S_z\cdot t + \frac{2k-1}{3(1-k)}\left[\left(\frac{d}{2}+t\right)^{\frac{3(1-k)}{2k-1}} - \left(\frac{d}{2}\right)^{\frac{3(1-k)}{2k-1}}\right] - \frac{2k+1}{2k-1}(p+S_z)\cdot t - \left[\frac{d}{2}\right]^{\frac{2}{2}}\right.$$

Gestopt met rekenen, omdat voor t nog in relatie met d ingevuld moet worden: $t = t_0\cdot\left(\frac{d}{d_0}\right)^{k-1}$, mits voor de eenvoud $\varepsilon_\varphi = \ln\frac{d+t}{d_0+t_0}$ gelijkgesteld wordt aan $\varepsilon_\varphi = \ln\frac{d}{d_0}$

Bovendien voldoet σ_r niet aan de tweede r.v.w.

We gaan over tot in eerder gedane veronderstelling

(B) σ_r is lineair verdeeld over de wand en voldoet aan

$\sigma_r\left(r=\frac{d}{2}\right) = -p$ en

$\sigma_r\left(r=\frac{d}{2}+t\right) = 0$; d.i. $\sigma_r = -p\left(1+\frac{d-2r}{2t}\right)$

lokaal e.w.: $\frac{d\sigma_r}{dr} + \frac{\sigma_r-\sigma_\varphi}{r} = 0$

$$\frac{p}{t} + \frac{1}{r}\left\{-p\left(1+\frac{d-2r}{2t}\right) - \frac{k+1}{2k-1}\left(-p\left(1+\frac{d-2r}{2t}\right)\right) + \frac{2-k}{2k-1}\cdot\sigma_z\right\} = 0$$

dus $\sigma_z = -p\left\{1 + \frac{d}{2t} + 3\frac{k-1}{2k}\cdot\frac{r}{t}\right\}$ en

$\sigma_\varphi = \frac{k+1}{2k-1}\cdot\sigma_r - \frac{2-k}{2k-1}\cdot\sigma_z = -p\left\{1+\frac{d-4r}{2t}\right\}$

$$F = 2\pi \int_{r=\frac{d}{2}}^{\frac{d}{2}+t} \sigma_z \cdot r\, dr = -\frac{\pi}{2} \cdot p \left\{ d^2 + 3dt + 2t^2 + 2 \cdot \frac{k-1}{2-k} \left(\frac{3}{2} d^2 + 3dt + 2t^2 \right) \right.$$

$$F_{pers} = F + -\frac{\pi}{4} d^2 \cdot p$$

$$\frac{F_{pers}}{p} = \frac{F}{p} - \frac{\pi}{4} d^2 = \frac{-\pi}{2(2-k)} \left[\left\{ \frac{2(2-k)}{4} + 2k - 1 \right\} d^2 + 3kdt + 2kt^2 \right]$$

Substitutie van $t = t_0 \left(\frac{d}{d_0} \right)^{k-1}$ levert

$$\boxed{\frac{F_{pers}}{p} = \frac{-\pi \cdot k}{4(2-k)} \left\{ 3 \cdot d^2 + 6 \cdot \frac{t_0}{d_0^{k-1}} \cdot d^k + 4 t_0^2 \cdot d_0^{2-2k} \cdot d^{-2+2k} \right\}}$$

(Opm.: vgl. met formule op blz. 9 met $k = 1$)

$$2\bar{\sigma}^2 = (\sigma_\varphi - \sigma_z)^2 + (\sigma_z - \sigma_r)^2 + (\sigma_r - \sigma_\varphi)^2 = 6 \left(\frac{pr}{t} \right)^2 \left(\frac{k^2 - k + 1}{(k-2)^2} \right)$$

$$\bar{\sigma} = C (\bar{\varepsilon} + \bar{\varepsilon}_0)^n \quad ; \quad \bar{\varepsilon} = \sqrt{\frac{2}{3}(\varepsilon_r^2 + \varepsilon_\varphi^2 + \varepsilon_z^2)} = \sqrt{\frac{4}{3}(k^2 - k + 1)} \cdot \varepsilon_\varphi$$

$$\text{dus} \quad p = -\frac{(k-2) \cdot t \cdot \bar{\sigma}}{r \sqrt{3(k^2 - k + 1)}} = \frac{(k-2) \cdot t}{r \sqrt{3(k^2 - k + 1)}} \cdot C \left[\bar{\varepsilon}_0 + \sqrt{\frac{4}{3}(k^2 - k + 1)}\, \varepsilon_\varphi \right]^n \quad [k$$

Neem aan dat $\varepsilon_\varphi = \ln \frac{d}{d_0}$ i.p.v. $\varepsilon_\varphi = \ln \frac{d+t}{d_0+t_0}$

$$\text{d.i.} \quad p\left(r = \frac{d}{2}\right) = -\frac{2(k-2) \cdot t_0 \left(\frac{d}{d_0} \right)^{k-1}}{d \sqrt{3(k^2 - k + 1)}} \cdot C \left[\bar{\varepsilon}_0 + \sqrt{\frac{4}{3}(k^2 - k + 1)} \ln \frac{d}{d_0} \right]^n$$

Het maximum van p treedt op voor $\frac{\partial p}{\partial d} = 0$

$$\Rightarrow \quad d_k = d_0 \exp \left\{ \frac{n}{2-k} - \frac{\bar{\varepsilon}_0}{\sqrt{\frac{4}{3}(k^2 - k + 1)}} \right\}$$

Programma ter berekening van F_{pers}, p en $\frac{F}{p}$ met grafiek uitvoer, zie bijlagen, op de HP gb25.
Tevens 3-D-grafiek ter verduidelijking waarom binnen de zwanehals bij $F_{pers} - p_{pomp}$-grafiek geblevn moet worden.

Knikgedrag

T.a.v. knik voor een cilinder onder inwendige druk is m. bekend, wel voor cilinders onder uitwendige druk (b.v. v drukboten). We beschouwen de cilinder zonder inwendige druk, maken gebruik van de elastische knikformule, er van uitgaande dat de diameter/wanddikte- en lengte/d meter-verhouding voldoende groot zijn en de oppervlakte gesteldheid aan de eisen voldoet. Het was mij te doen om een globale uitspraak over het knikgedrag van de cilinder onder de berekende belasting. Daarb heb ik gebruik gemaakt van twee artikeltjes, te weten: "A design approach for axially compressed unstiffened cylinders" en "Buckling behaviour of plate and shell structures" (zie bijlagen). M.b.v. fig. 3 op blz. 386 1/4 eerste bijlage heb ik een aantal belastingparameters λ uitgerekend voor de verschillende gewenste diameters 1/4 cilinder in het proces, waarbij $k=1$, $n=0{,}08$, $\bar{\varepsilon}_0=0{,}036$, $C=52$, $E=210.000\ N/mm^2$, $\nu=0{,}3$, $t_0=3$ mm. en vergeleke met de figuur, hoewel dat helemaal niet mag, omdat de geometrie van de cilinder gekenmerkt wordt door $L/R=2{,}00$ en $R/t=300$, terwijl onze cilinder in de loop 1/4 proces in L/R ondergaat van $24 \rightarrow 15$ en een R/t " " $10 \rightarrow 23$

$$\lambda = \frac{P(1-\nu^2)\cdot t_0^3}{2\pi \cdot R \cdot E \cdot t} \qquad R=\frac{d}{2},\ P=-F,\ t=t_0\left(\frac{d}{d_0}\right)^{-k}=t_0$$

Daarnaast is λ ook berekend met voor $E=E^*$.

$$\frac{d\bar{\varepsilon}}{d\bar{\varepsilon}} = C\cdot n\,\bar{\varepsilon}^{\,n-1} = C\cdot n\left(\ln\frac{d}{d_0}\right)^{n-1} \rightarrow \lambda^*$$

d [mm]	p [N/mm²]	λ [-]	$\lambda^* = \lambda \cdot \frac{E}{E^*}$ [-]	E^* [N/
60	23,01	1,1467	∞	0
60,1	23,07	1,1513	16,146	14.994
63	23,63	1,2288	–	~~222~~ –
65	23,52	1,2570	–	~~109~~ –
70	22,75	1,2980	1167	~~95~~ 23
80	20,79	1,3363	2142	~~23~~ 13
90	18,95	1,3549	2995	~~66~~ 95
100	17,35	1,3658	3725	~~88~~ 77
110	15,98	1,3734	4370	66
120	14,80	1,3789	4993	58
130	13,77	1,3824	5477	53
140	12,88	1,3860	6064	48

$$\lambda = \frac{(1-\nu^2)\cdot w^3}{E} \cdot \frac{p}{2}\left(3 + \frac{d}{t_0} + \frac{2t_0}{d}\right)$$

Passen we de gevonden waarden in in fig. 3, er van uitgaande dat de R/t en L/R - waarden er even niets toe doen, dan zien we dat volgens klassieke theorie en elasticiteitsmodulus E, de cilinder niet zal knikken maar volgens de nieuwe benadering wel en zeker voor de 'plasticiteitsmodulus' E^* zal knikken.
Zoals ook uit de proeven blijkt knikt de pijp. Tange volge hiervan deformeert de pijp niet zoals we willen. Het is zelfs zo, dat de verwachte versteviging uitblijft opdat de rest van de pijp op diameter zou kunnen komen. In de toekomst moet hiermee terdege rekening worden gehouden. De Eulerse knik is niet te voorkomen, door in het begin de druk relatief

hoog te houden.

Model, waarbij al een bolvormige ring is ontstaan.

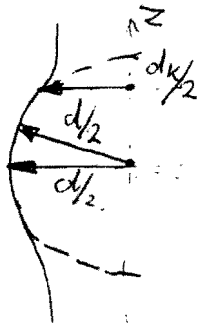

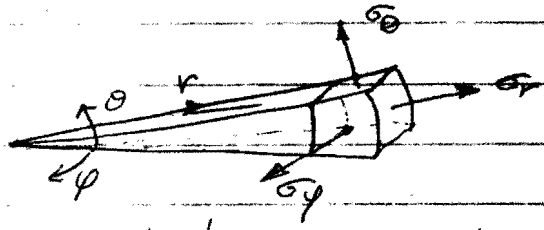

dit zijn de hoofdspanningsrichtingen, dus

$\sigma_{r\varphi} = \sigma_{r\theta} = \sigma_{\theta\varphi} = 0$.

Lokaal e.w. :

$$\frac{\partial \sigma_r}{\partial r} + \frac{1}{r}(2\sigma_r - \sigma_\theta - \sigma_\varphi) = 0$$

$$\frac{1}{r}\frac{\partial \sigma_\theta}{\partial \theta} + \frac{1}{r}(\sigma_\theta - \sigma_\varphi)\cot\theta = 0$$

$$\frac{1}{r\sin\theta}\frac{\partial \sigma_\varphi}{\partial \varphi} = 0 \rightarrow \sigma_\varphi \neq \sigma_\varphi(\varphi)$$

Neem voor $\sigma_r = -p\left\{1 + \frac{d-2r}{2t}\right\}$ aan

d.i. $\frac{1}{r}(\sigma_\theta + \sigma_\varphi) = \frac{\partial \sigma_r}{\partial r} + \frac{2}{r}\sigma_r \Rightarrow \sigma_\theta + \sigma_\varphi = \frac{p}{t}\{3r - 2t - d$

dus $\sigma_\varphi = -\sigma_\theta + \frac{p}{t}(3r - 2t - d)$; substitutie hiervan in de tweede vgl. v/h Lokaal e.w. levert:

$$\frac{1}{r}\left\{\frac{\partial \sigma_\theta}{\partial \theta} + 2\sigma_\theta \cot\theta - \frac{p}{t}(3r - d - 2t)\cot\theta\right\} = 0$$

Homogene D.V. : $\frac{\partial \sigma_\theta}{\partial \theta} = -2\sigma_\theta \cot\theta \Rightarrow \sigma_{\theta_h} = \frac{C}{\sin^2\theta}$ $(\theta \neq$

particuliere oplossing : $\sigma_{\theta_p} = \frac{p}{2t}(3r - d - 2t)$

d.i. $\sigma_\theta = \sigma_{\theta_p} + \sigma_{\theta_h} = \frac{C}{\sin^2\theta} + \frac{p}{2t}(3r - d - 2t)$ $(\theta \neq 0)$

d.i. $\sigma_\varphi = \frac{-C}{\sin^2\theta} + \frac{p}{2t}(3r - 2t - d)$

$$2\bar{\sigma}^2 = (\sigma_r - \sigma_\varphi)^2 + (\sigma_\varphi - \sigma_\theta)^2 + (\sigma_\theta - \sigma_r)^2 = \frac{6C^2}{\sin^4\theta} + \frac{p^2 r^2}{2t^2}$$

L.v.M. :

$$\varepsilon_r = \frac{\bar{\varepsilon}}{\bar{\sigma}}\left(\sigma_r - \frac{\sigma_\varphi + \sigma_\theta}{2}\right) = \frac{\bar{\varepsilon}}{\bar{\sigma}}\,\frac{-pr}{2t}$$

$$\varepsilon_\varphi = \frac{\bar{\varepsilon}}{\bar{\sigma}}\left(\sigma_\varphi - \frac{\sigma_r + \sigma_\theta}{2}\right) = \frac{\bar{\varepsilon}}{\bar{\sigma}}\left[-\frac{3}{2}\,\frac{C}{\sin^2\theta} + \frac{p\cdot r}{4t}\right]$$

$$\varepsilon_\theta = \frac{\bar{\varepsilon}}{\bar{\sigma}}\left(\sigma_\theta - \frac{\sigma_r + \sigma_\varphi}{2}\right) = \frac{\bar{\varepsilon}}{\bar{\sigma}}\left[\frac{3}{2}\,\frac{C}{\sin^2\theta} + \frac{p\cdot r}{4t}\right]$$

Bepaling van de constante C :

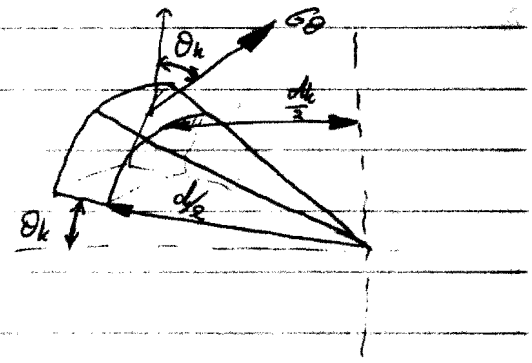

Op $\frac{d_k}{2}$ verlaat de buis de bolvorm en gaat over in cilindervorm.

Globaal e.w. : $\cos\theta_k = \frac{d_k}{d}$; d.i. $\sin\theta_k = \sqrt{1-\left(\frac{d_k}{d}\right)^2}$

$$\int_{A_{\theta_1}} \sigma_\theta \cos\theta_k \, dA_{\theta_1} = \int_{A_{\theta_2}} \sigma_2 \, dA_{\theta_2} \quad ; \quad \int_{A_{\theta_2}} dA_{\theta_2} = \int_0^{2\pi} r\,d\varphi \int_{r=\frac{d_k}{2}}^{\frac{d_k}{2}+t} d$$

$$\int_0^{2\pi} r\,d\varphi \int_{r=\frac{d}{2}}^{\frac{d}{2}+t} \left[\frac{C}{\sin^2\theta} + \frac{p}{2t}(3r - d - 2t)\right]\cos\theta_k \, dr = \int_0^{2\pi} r\,d\varphi \int_{r=\frac{d_k}{2}}^{\frac{d_k}{2}+t} -p\left\{1 + \frac{d}{2t} + 3\,\frac{\frac{k-1}{2-k}\,\frac{r}{t}}{}\right.$$

daaruit volgt: $C = \frac{(d^2 - d_k^2)\,p}{2\cdot d\cdot d_k\cdot t(d+t)}\left\{-\frac{3}{2}d_k\cdot d - \left(2 + 6\,\frac{k-1}{2-k}\right)d_k\cdot t - d\cdot t - \left(\frac{k-1}{2-k}\right)3t^2\right.$

$$\left.\left(2 + 4\left(\frac{k-1}{2-k}\right)\right)\cdot t^2\right\}$$

Verwaarloos de termen t^2, $d_k\cdot t$ en $d\cdot t$ en neem $k = 1$

d.i. $C = -\frac{3}{4}\,\frac{(d^2 - d_k^2)}{t(d+t)}\,p$

daaruit volgt voor de spanningen :

$$\sigma_r = \frac{p}{2t}(2r-d-2t)$$

$$\sigma_\varphi = \frac{p}{2t}(3r-d-2t) + \frac{3}{4}\frac{(d^2-d_k^2)\cdot p}{t(d+t)\sin^2\theta}$$

$$\sigma_\theta = \frac{p}{2t}(3r-d-2t) - \frac{3}{4}\frac{(d^2-d_k^2)\,p}{t(d+t)\sin^2\theta}$$

$$\bar{\sigma}^2 = \frac{1}{4}\left\{ \frac{27}{4}\frac{(d^2-d_k^2)^2\cdot p^2}{t^2(d+t)^2\sin^4\theta} + \frac{p^2\cdot r^2}{t^2} \right\}$$

$\bar{\sigma}$ treedt het eerst op voor $r = \frac{d}{2}+t$ en $\theta \to 0$

$$\sigma_\theta\left(r=\frac{d}{2}+t\right) = 0 \quad \text{als} \quad \frac{p}{2t}\left(\frac{3}{2}d+3t-d-2t\right) = \frac{6}{4}\frac{(d^2-d_k^2)\,p}{t(d+t)\sin^2\theta}$$

dus als $\sin\theta = \sqrt{\frac{3(d^2-d_k^2)}{(d+t)(d+2t)}} \approx \sqrt{3}\cdot\sqrt{1-\left(\frac{d_k}{d}\right)^2} = \sqrt{3}\cdot\sin\theta_k$

~~$\Rightarrow$ bij $\theta = \theta_k$ zal het eerst een trekspanning optreden~~
d.w.z. dat voor $\theta > \theta_k$ 'n trekspanning optreedt maar daar volgens de geometrie $\theta \leq \theta_k$ zal dus altijd 'n drukspanning in de θ-richting heersen mits de axiale kracht overal 'n functie van p voorstelt aangebracht.

#

Opmerkingen:

F_{pers} > als of $K >$ of $n <$ of $\varepsilon_0 >$ of t

p_{comp} > als of $K <$ of $n <$ of $\varepsilon_0 >$ of t

$\frac{F_{pers}}{p}$ alleen afhankelijk van K en wordt groter als $K >$ wordt.

```
0: "Lantaarnpaal
 -Jan Vosmer dd
 mrt 82":
1: ent "0 |tekst
 ",J;if J=0;prt
 "FILE 26; Opbla
 zen lantaarnpaa
 l"
2: dim D[0:40],
 P[0:40],F[0:40]
 ,V[0:40],M[0:40
 ],R[0:18]
3: 60→r1;140→r2;
 11→r10;0→r11;
 7→r12;27→r20;
 100→r110;700→r1
 20
4: pclr;wrt 705,
 "ip 520,380,
 7720,10380"
5: ent "C-waarde
 ?",C,"verstevig
 ingsexponent?",
 N,"voordeformat
 ie?",E
6: ent "wanddikt
 e pijp?",T,"pij
 pbinnendiameter
 ?",O
7: ent "1 |berek
 ening F,P,V",J;
 if J#1;jmp 22
8: ent "rekwegfa
 ctor",K
9: for I=0 to 40
10: 60+2*I→D[I]
11: next I
12: for I=0 to
 40
13: if E=0 and
 I=0;gto 23
14: (E+r(4*(K↑2-
 K+1)/3)*ln(D[I]
 /O))↑N*2*C*(2-
 K)*T*(D[I]/O)↑(
 K-1)→A
15: A/(D[I]*r(3*
 (K↑2-K+1)))→P[I
 ]
16: π*K*(3*D[I]↑
 2+6*T*D[I]↑K/
 O↑(K-1)+4*T↑2*
 O/D[I])/(4*(2-
 K))→V[I]
17: V[I]*P[I]→F[
 I]
18: next I
19: if E=0;F[1]→
 F[0];P[1]→P[0];
 V[1]→V[0]
20: ent "1 |prin
 ten invoer",J;
 if J#1;jmp 3
21: fxd 3;prt
 "C-waarde= ",C,
 "versteviginge
 xponent= ",N,
 "voordeformatie
 = ",E
22: prt "rekwegf
 actor= ",K,"wan
 ddikte= ",T,
 "pijpdiameter=
 ",O
23: ent "1 |prin
 ten uitvoer",J;
 if J#1;jmp 3
24: for I=0 to
 40 by 4;prt
 D[I],V[I]/10↑4,
 P[I],F[I]/1000
25: next I
26: ent "1 om
 assen te tekene
 n",J;if J=1;
 cll 'assen'
27: ent "1 om
 functie te teke
 nen",J;if J=1;
 cll 'functie'
28: ent "1 voor
 nog een functie
 ",J;if J=1;jmp
 -1
29: ent "2 om
 assen2 te teken
 en",J;if J=2;
 cll 'assen2'
30: ent "2 om
 functie2 te
 tekenen",J;if
 J=2;cll 'functi
 e2'
31: ent "2 |bere
 kening instabie
 l",J;if J#2;
 jmp 10
32: .9→K;for
 I=0 to 40
33: (40-I)*.9/
 40→K;0*exp(N/
 (1-K))→D[I]
34: (E+r(4*(K↑2-
 K+1)/3)*ln(D[I]
 /O))↑N*2*C*(2-
 K)*T*(D[I]/O)↑(
 K-1)→A
35: A/(D[I]*r(3*
 (K↑2-K+1)))→P[I
 ]
36: π*K*(3*D[I]↑
 2+6*T*D[I]↑K/
 O↑(K-1)+4*T↑2*
 O/D[I])/(4*(2-
 K))→V[I]
37: V[I]*P[I]→F[
 I]
38: next I;ent
 "2 |printen
 instabiel",J;
 if J#2;jmp 3
39: for I=0 to
 40 by 5;prt
 D[I],V[I]/10↑4,
 P[I],F[I]/1000
40: next I
41: ent "1 |prin
 ten uitvoer",J;
 if J#1;jmp 3
42: fxd 3;prt
 "C-waarde= ",C,
 "versteviginge
 xponent= ",N,
 "voordeformatie
 = ",E
43: prt "wanddik
 te= ",T,"pijpdi
 ameter= ",O
44: ent "1 om
 assen te tekene
 n",J;if J=1;
 cll 'assen'
45: ent "1 om
 een functie te
 tekenen",J;if
 J=1;gsb "functi
 e"
46: ent "1 voor
 nog een functie
 ",J;if J=1;jmp
 -1
47: ent "2 om
 assen2 te teken
 en",J;if J=2;
 gsb "assen2"
48: ent "2 om
 functie2 te
 tekenen",J;if
 J=2;gsb "functi
 e2"
```

```
49: stp
50: "assen":
51: pen# 4
52: scl (r1*16-
 r2)/15,r2,1.1*
 r11-.1*r12,r12
53: fxd 0
54: xax r11,5,
 r1,r2,2
55: fxd 1
56: yax r1,.5,
 r11,r12,1
57: pen
58: ret
59: "functie":
60: ent "Welke
 pen ?",J
61: if J>8 or
 J<0;pen# 4;jmp
 2
62: pen# J
63: ent "Welk
 lijntype ?",J
64: if J>6 or
 J<0;line ;jmp 2
65: line J
66: ent "Welke
 fie ?, 1=V,
 2=F, 3=P",J
67: if J=2;for
 I=0 to 40;F[I]/
 10↑5→M[I];next
 I;jmp 3
68: if J=3;for
 I=0 to 40;P[I]/
 10→M[I];next I;
 jmp 2
69: for I=0 to
 40;V[I]/10↑4→M[
 I];next I
70: pen
71: plt D[0],
 M[0],-2
72: for I=1 to
 40
73: plt D[I],
 M[I],0
74: next I
75: ptyp
76: pen# 0
77: ret
78: "assen2":
79: pen# 4
80: scl r10+(r10
 -r20)/8,r20,
 r110+(r110-r120
 )/24,r120
81: fxd 0
82: xax r110,1,
 r10,r20,2
83: yax r10,50,
 r110,r120,1
84: pen
85: ret
86: "functie2":
87: ent "Welke
 pen ?",J
88: if J>8 or
 J<0;pen# 4;jmp
 2
89: pen# J
90: ent "Welk
 lijntype ?",J
91: if J>6 or
 J<0;line ;jmp 2
92: line J
93: pen
94: plt P[0],
 F[0]/1000,-2
95: for I=1 to
 40
96: plt P[I],
 F[I]/1000,0
97: next I
98: ptyp
99: pen# 0
100: ret
*15615
```

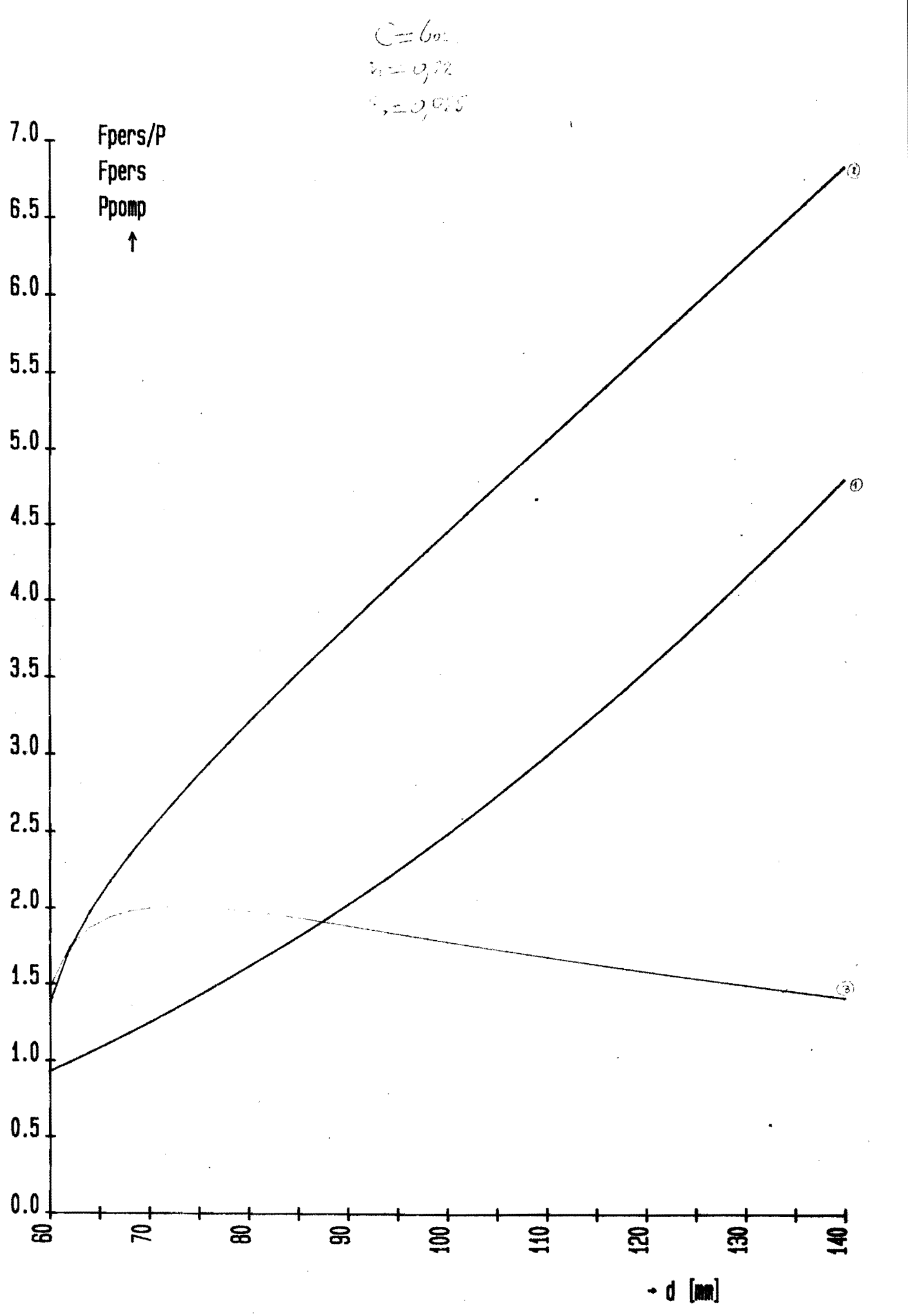
C=60
η=0,92
η=0,915
7.0
6.5
6.0
5.5
5.0
4.5
4.0
3.5
3.0
2.5
2.0
1.5
1.0
0.5
0.0
Fpers/P
Fpers
Ppomp
↑
①
②
③
60
70
80
90
100
110
120
130
140
→ d [mm]

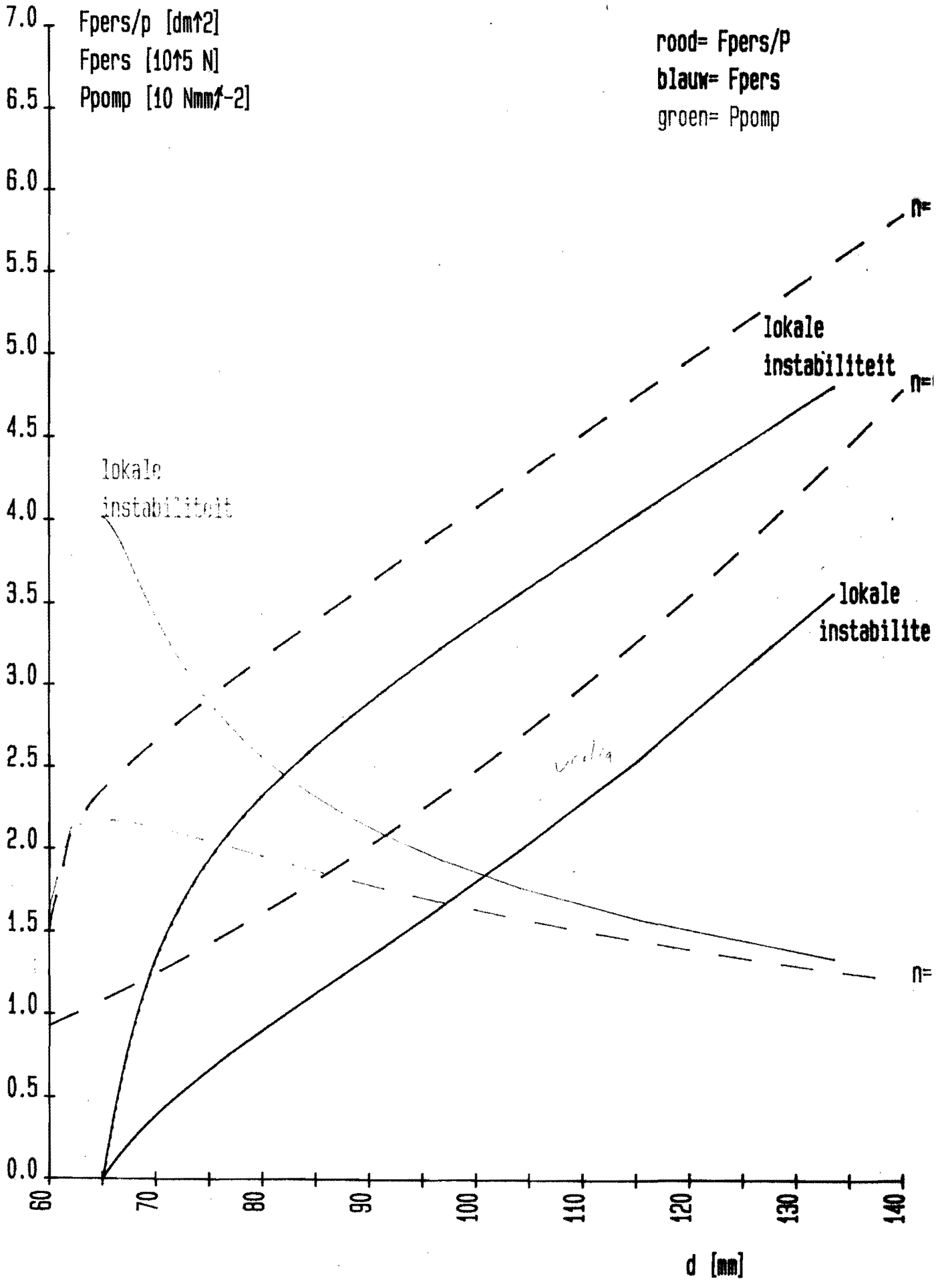
Fpers/p [dm↑2]
Fpers [10↑5 N]
Ppomp [10 Nmm↑-2]
rood= Fpers/P
blauw= Fpers
groen= Ppomp
lokale instabiliteit
lokale instabiliteit
lokale instabilite
n=
n=
n=
7.0
6.5
6.0
5.5
5.0
4.5
4.0
3.5
3.0
2.5
2.0
1.5
1.0
0.5
0.0
60
70
80
90
100
110
120
130
140
d [mm]

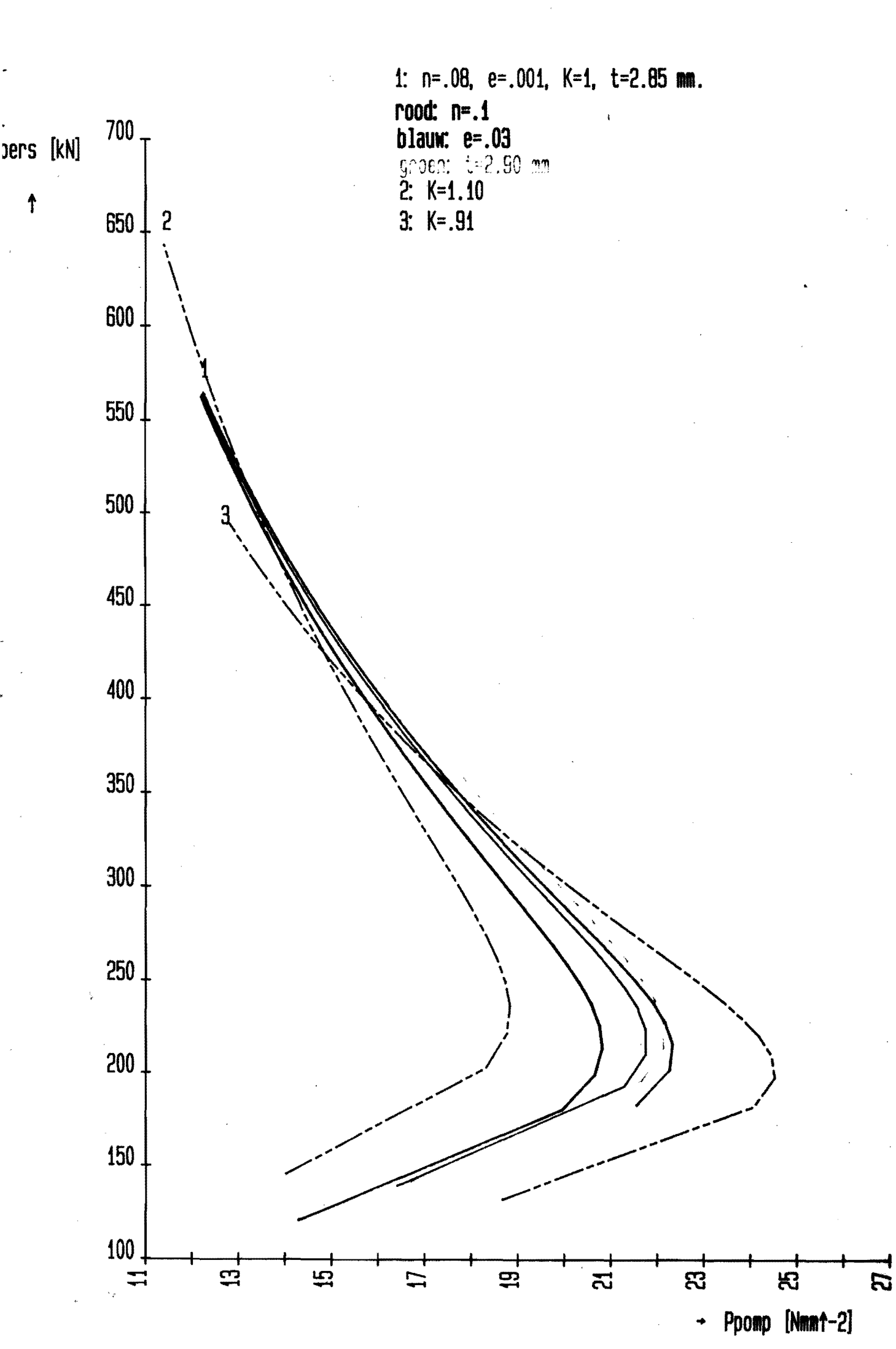
1: n=.08, e=.001, K=1, t=2.85 mm.
rood: n=.1
blauw: e=.03
groen: t=2.90 mm
2: K=1.10
3: K=.91
pers [kN]
↑
700
650
600
550
500
450
400
350
300
250
200
150
100
11
13
15
17
19
21
23
25
27
→ Ppomp [Nmm↑-2]

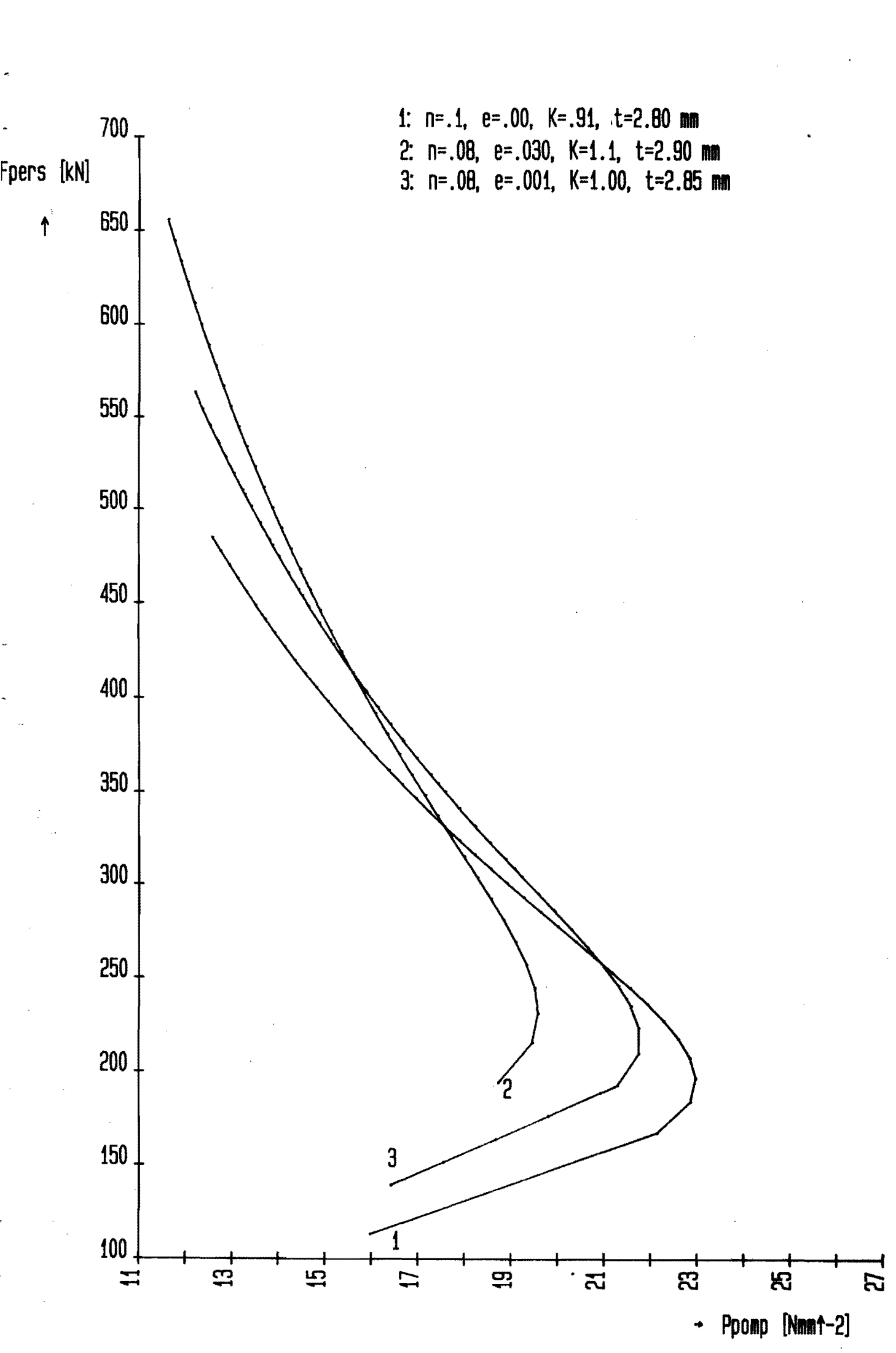
1: n=.1, e=.00, K=.91, t=2.80 mm
2: n=.08, e=.030, K=1.1, t=2.90 mm
3: n=.08, e=.001, K=1.00, t=2.85 mm
Fpers [kN]
700
650
600
550
500
450
400
350
300
250
200
150
100
11
13
15
17
19
21
23
25
27
Ppomp [Nmm↑-2]
1
2
3

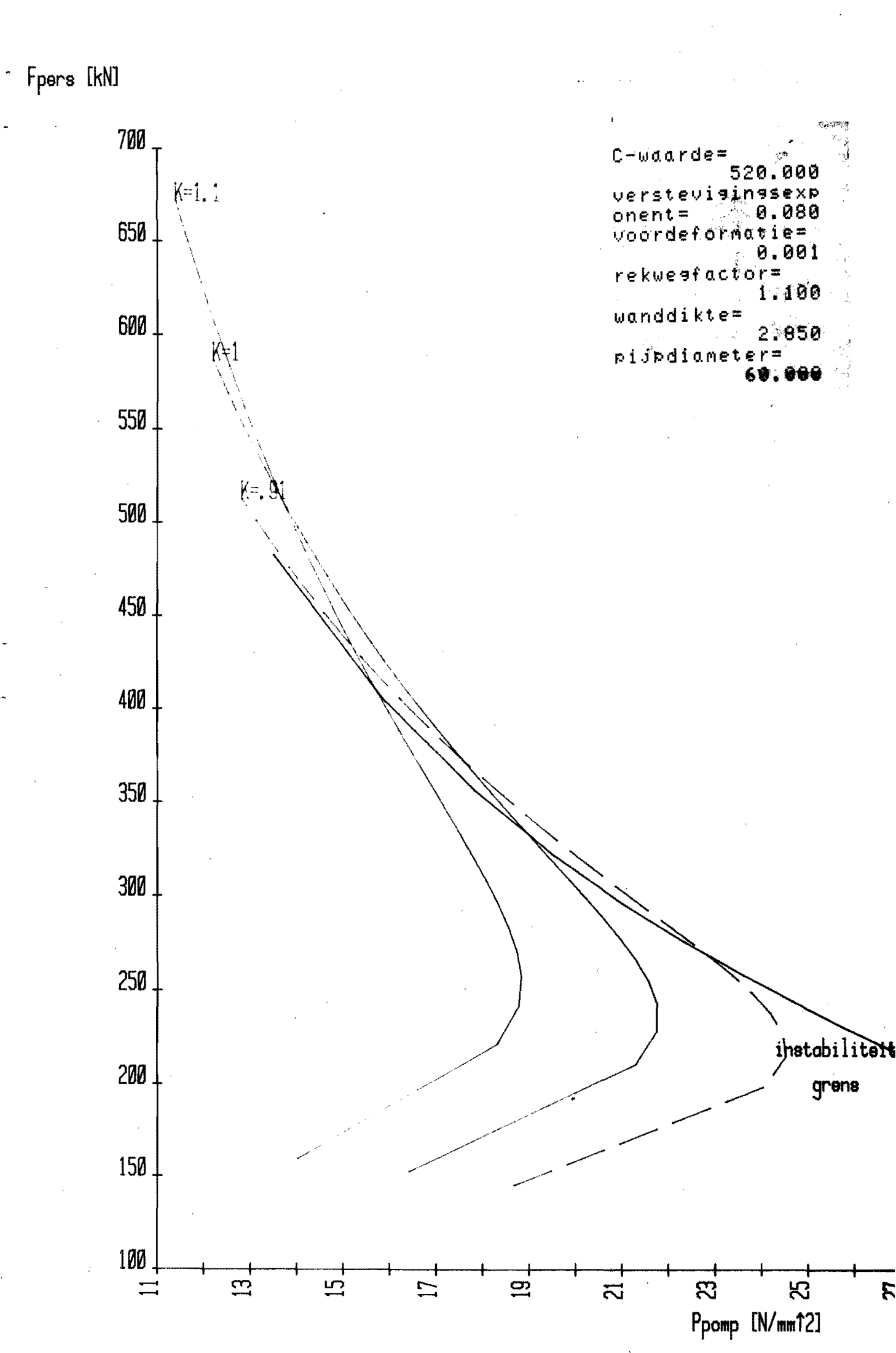
Fpers [kN]
700
650
600
550
500
450
400
350
300
250
200
150
100
K=1.1
K=1
K=.9
C-waarde=
520.000
verstevigingsexponent=
0.080
voordeformatie=
0.001
rekwegfactor=
1.100
wanddikte=
2.850
pijpdiameter=
60.000
instabiliteit
grens
11
13
15
17
19
21
23
25
Ppomp [N/mm↑2]

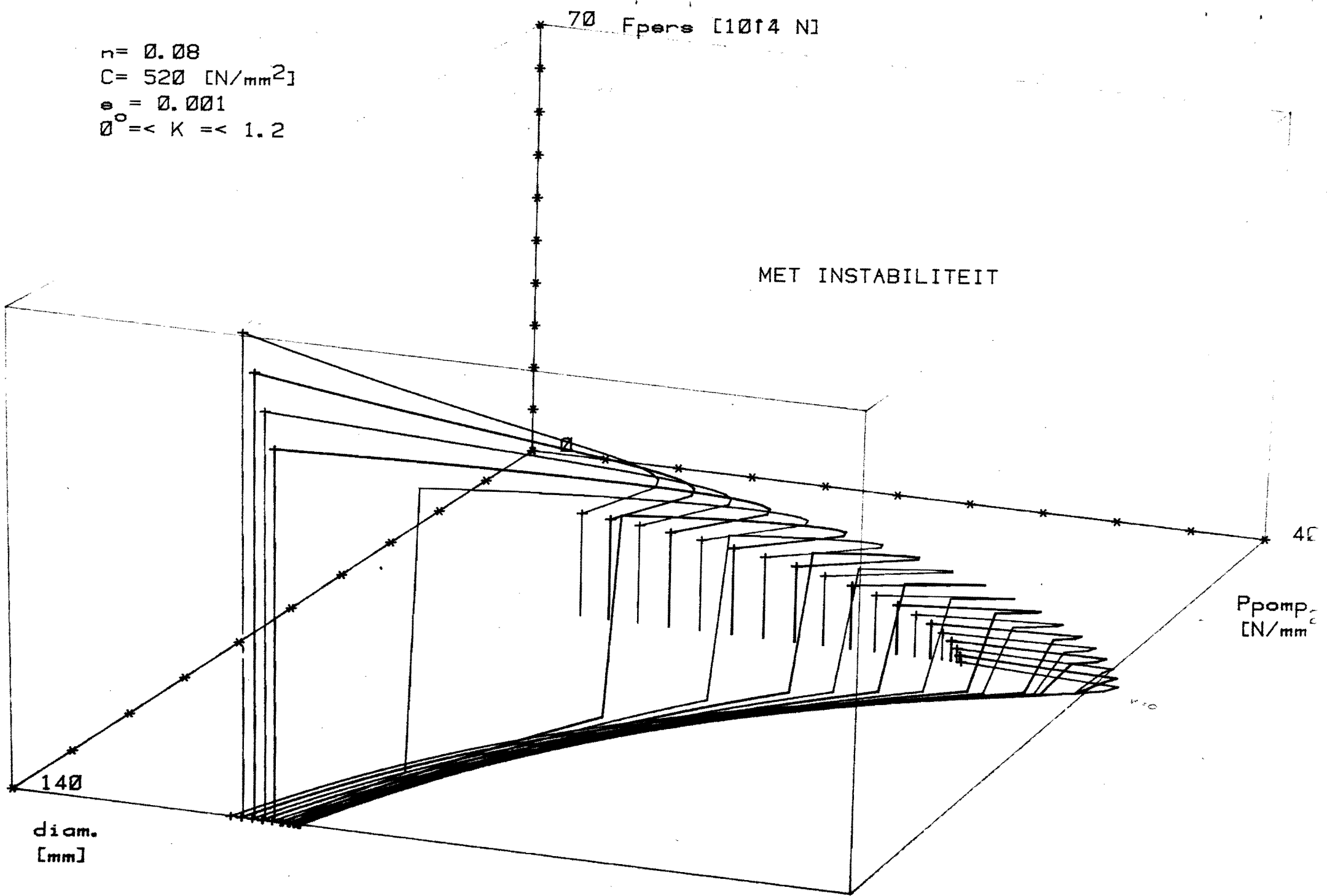
n= 0.08
C= 520 [N/mm2]
e = 0.001
0°=< K =< 1.2
70 Fpers [10↑4 N]
MET INSTABILITEIT
0
40
Ppomp
[N/mm
140
diam.
[mm]

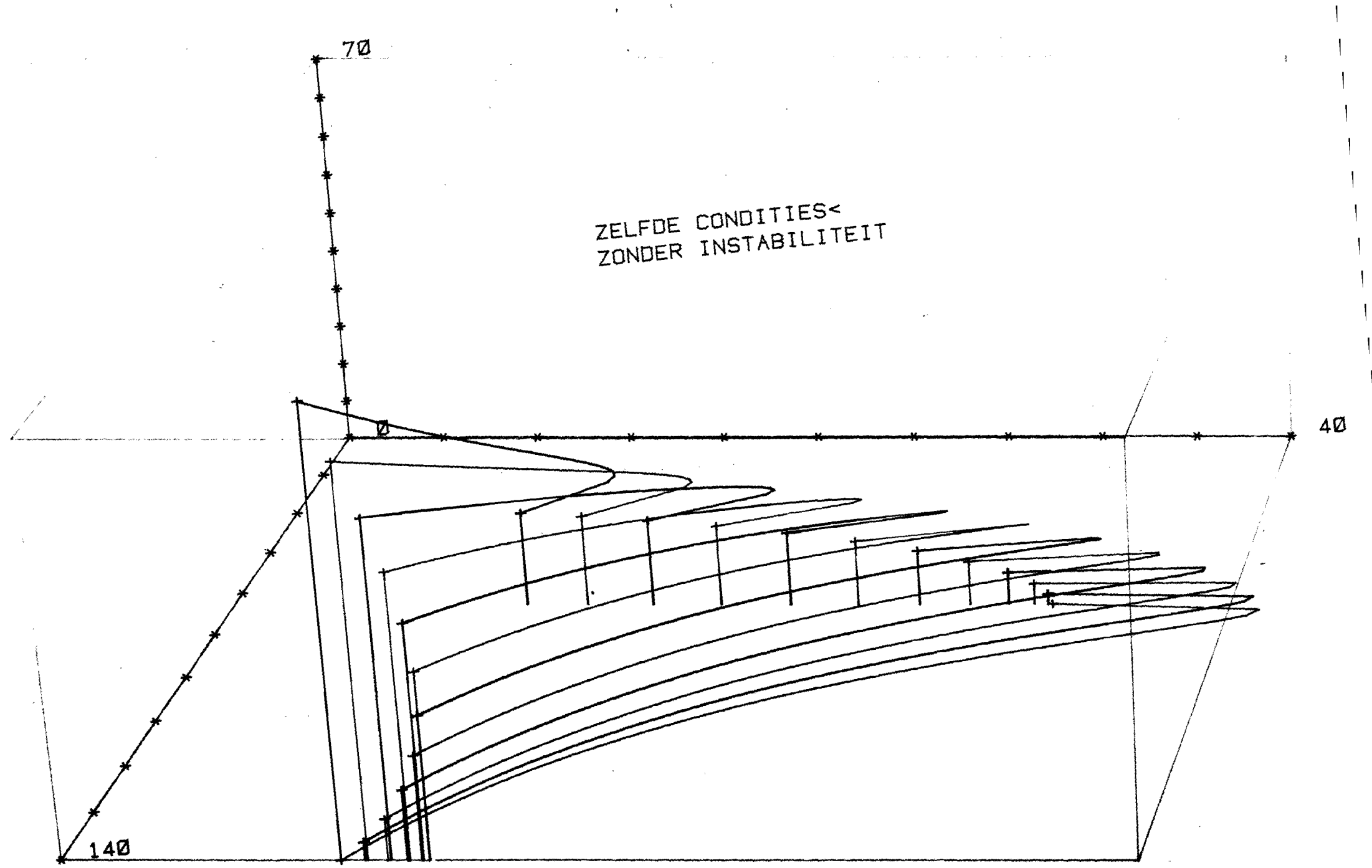
70
ZELFDE CONDITIES<
ZONDER INSTABILITEIT
0
40
140

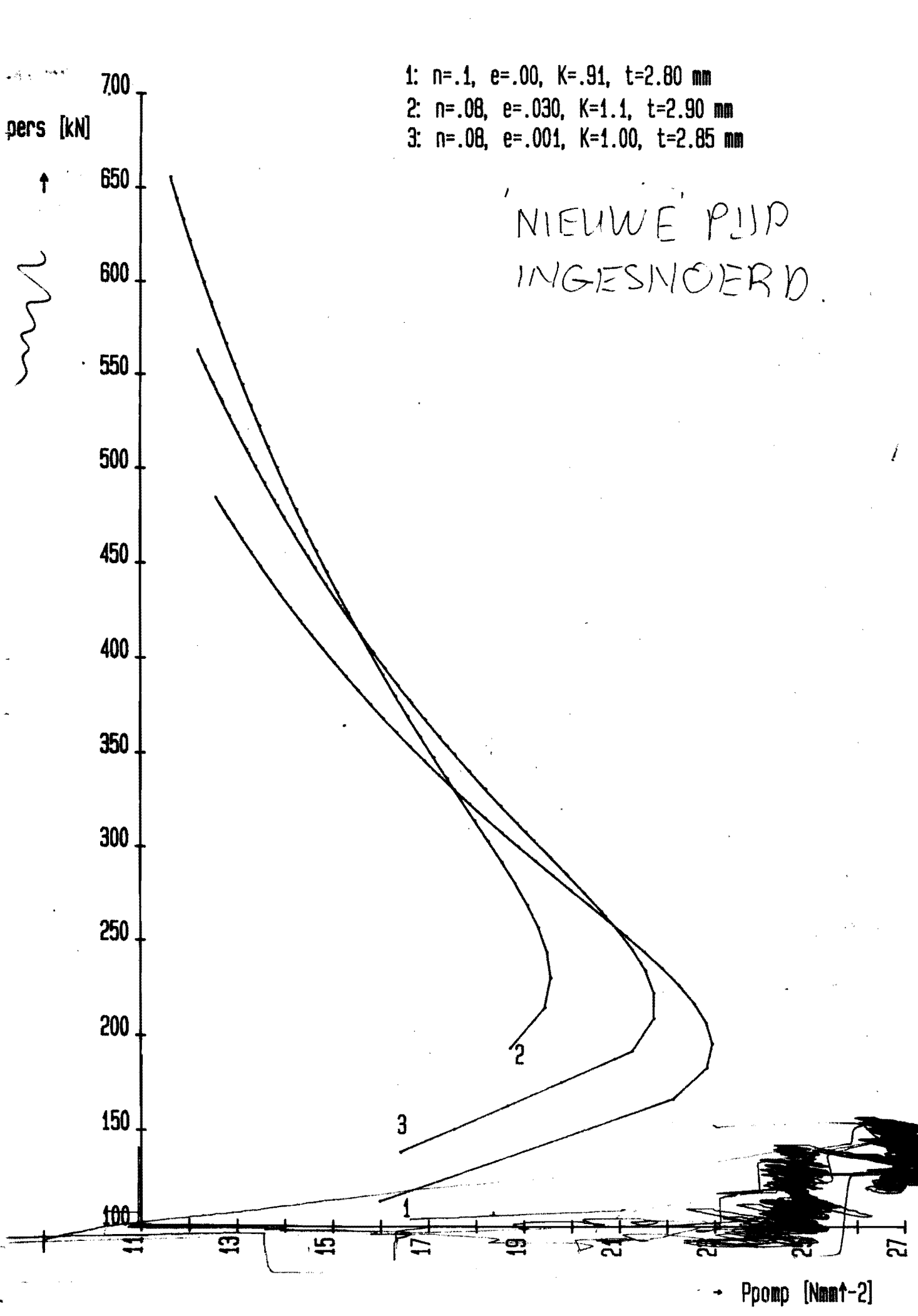
1: n=.1, e=.00, K=.91, t=2.80 mm
2: n=.08, e=.030, K=1.1, t=2.90 mm
3: n=.08, e=.001, K=1.00, t=2.85 mm
NIEUWE PIJP
INGESNOERD
pers [kN]
700
650
600
550
500
450
400
350
300
250
200
150
100
11
13
15
17
19
21
23
25
27
Ppomp [Nmm↑-2]
1
2
3

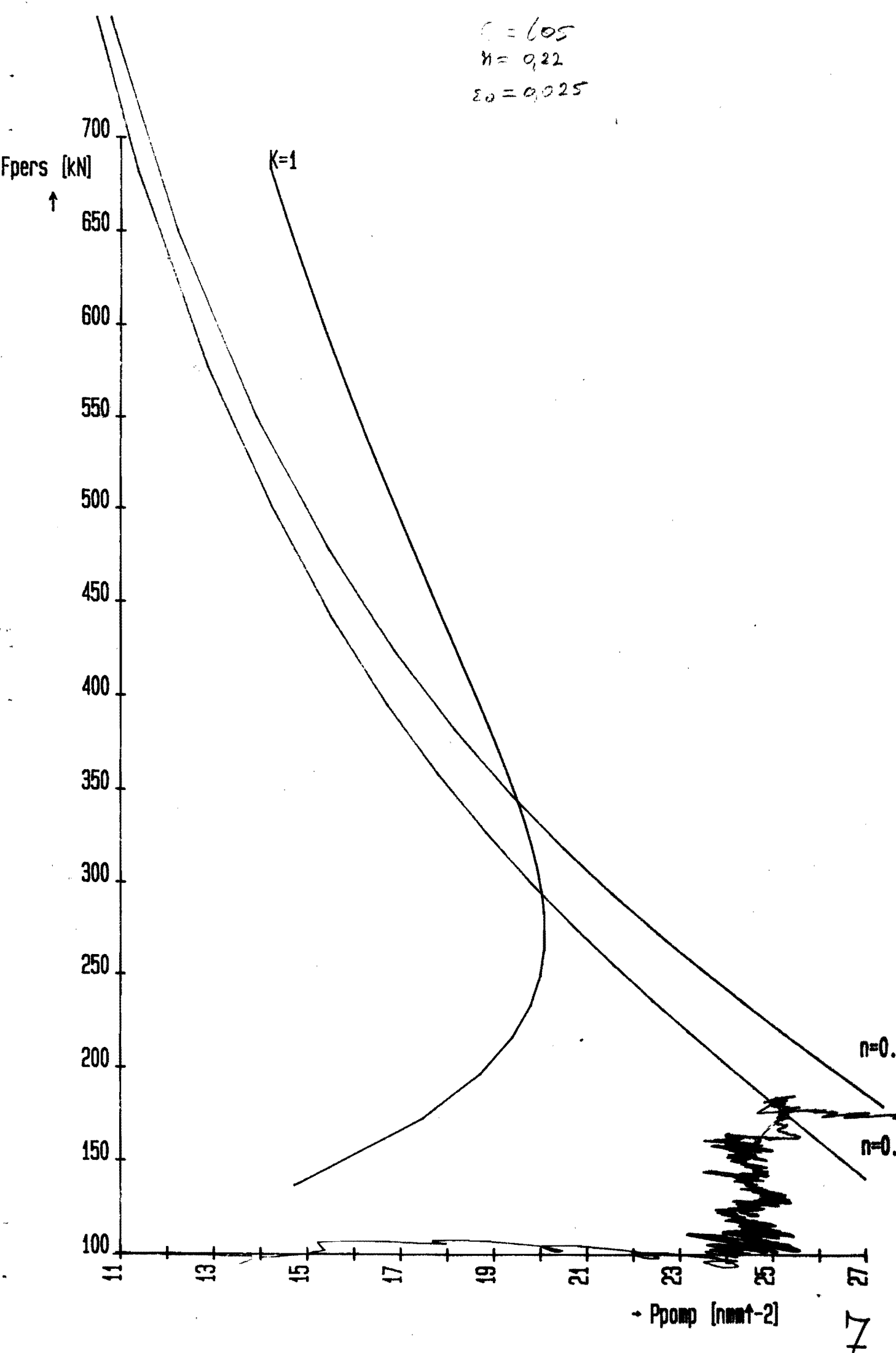
C = 605
n = 0,22
ε0 = 0,025
Fpers [kN]
700
650
600
550
500
450
400
350
300
250
200
150
100
K=1
n=0.
n=0.
11
13
15
17
19
21
23
25
27
→ Ppomp [nmm↑-2]

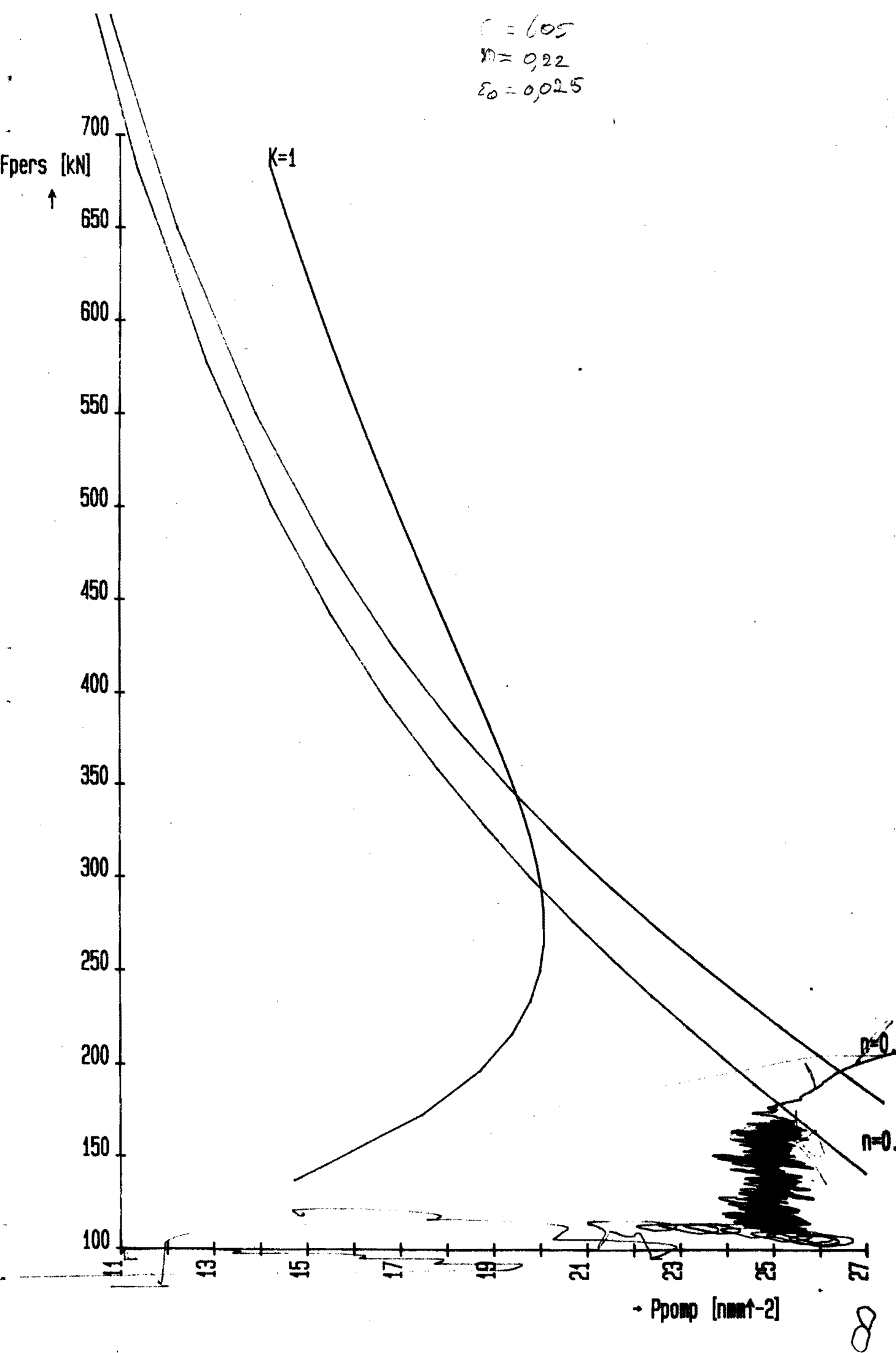
C = 605
n = 0,22
ε0 = 0,025
Fpers [kN]
700
650
600
550
500
450
400
350
300
250
200
150
100
K=1
11
13
15
17
19
21
23
25
27
→ Ppomp [nmm↑-2]
p=0
n=0.

Conclusies

- Uit de proeven is gebleken, dat een lage verstevigingsexponent de voorkeur verdient, dit is in tegenstelling met de uitleg bij de foto's (foto @ met $n = 0.22$ en foto © met $n = 0,08$). Nadere beschouwing vereist
- Als 'tegen' de grenservormingskromme aan gedeformeerd wordt blijken de axiale spanningen nog te hoog te zijn en dus treedt knik op. Opgemerkt dient wel te worden, dat de conciteit erg groot was in de proeven, waardoor het materiaal de gelegenheid aangenomen werd om aan te gaan leggen en zodoende het knikgedrag te beperken.
- Fpers / $\frac{1}{4}\pi d^2$ in de druk is in feite geen juiste maat voor de vervorming. indien knik optreedt, doet ook niet als knik zich niet voordoet. De diameter dient wel degelijk als parameter nodig te zijn. Zie dwarsdoorsnede grafiek. Een juiste grafiek om het proces te volgen zou zijn de verhouding van Fpers en de paalpotentiaal als functie van de diameter en daarin aangegeven de grenzen waarbinnen gebleven moet worden.
- Het produceren van een conische pijp in één keer zal voorlopig niet mogelijk zijn; doch gedacht moet worden aan een eenheid, waarin het proces plaatsvindt, die langs de pijp 'loopt'
- Voor een juiste beschrijving van de theorie zou niet lineair plasticiteitsmechanica gehanteerd dienen te wor

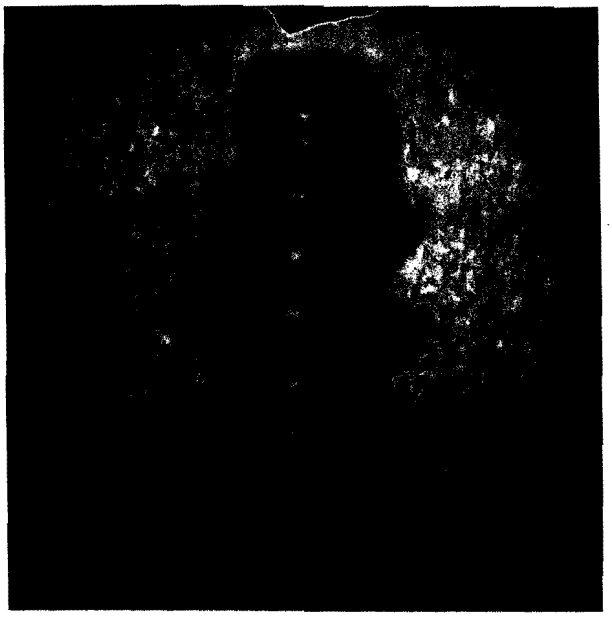

(a)

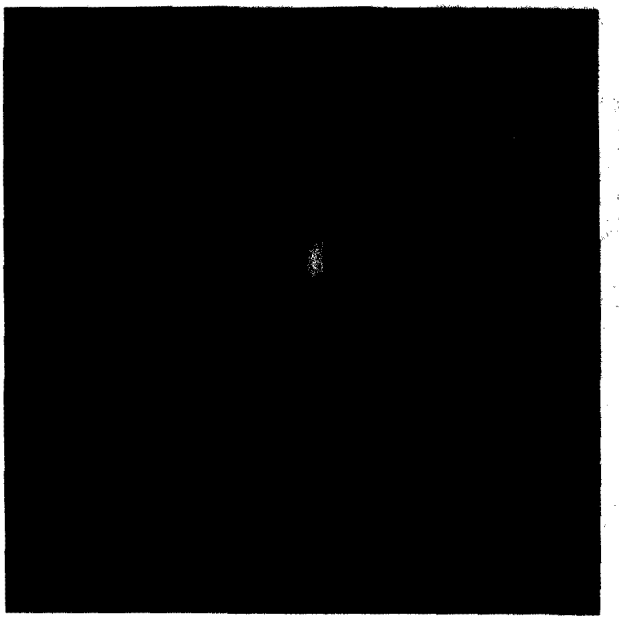

(b)

(c)

(a) De elastische knik vorm duidelijk aanleiding om op de knikplaatsen plastisch te deformeren. De verschuiving ($n = 0,22$) is onvoldoende om de ringen te doen stabiliseren en vervolgens de rest v/h materiaal mee te laten doen.

(b) Aan de insnoering is te zien dat de spanningsweerstand aardig benaderd is.

(c) Hier zijn ook eerst ringen gevormd en vervolgens na verschuiving is de rest v/h materiaal meegekomen.

7. HARDING, J. E., HOBBS, R. E. and NEAL, B. G., Ultimate load behaviour of plates under combined direct and shear in-plane loading, *Steel Plated Structures; an International Symposium*, Crosby Lockwood Staples, London, 1977.
8. HARDING, J. E. and HOBBS, R. E., *The ultimate load behaviour of box girder web panels*. Submitted for publication.
9. HORNE, M. R., DOWLING, P. J. and OGLE, M. H., *Report to Steering Group on Plated Structures*, Committee B116/3, British Standards Institution, London, England, 1976.

21

A Design Approach for Axially Compressed Unstiffened Cylinders

R. C. BATISTA†
Universitade Federal do Rio de Janeiro

AND

J. G. A. CROLL
University College, London

SUMMARY

The classical critical load analysis of circular cylindrical shells under the action of uniform axial compression is re-examined. It is shown, through the inspection of the potential energy, which of the components of the membrane stiffness are most likely to be eroded during the imperfection-sensitive, non-linear mode interaction that occurs in the buckling of these shells. Based upon this reassessment a simplified critical load analysis is outlined which, in contrast with the classical theory, is shown to predict a critical load associated with a unique critical mode that appears to agree with the buckling modes observed in both the present experimental programme and those described in the literature.

Apart from providing close agreement with observed buckling modes, the simplified theory is shown to have other advantages which should commend it to the designer. First, in contrast with other theories to account for its 'perplexing behaviour', the present simplified theory does not involve the lengthy solution of highly non-linear equations. Second, and possibly most significant, when proper account is taken of all the appropriate parameters describing the behaviour of the shell, the method provides lower bound estimates of reported buckling loads. Properly extended therefore, the method could provide the basis of a simple but safe design procedure.

† Presently engaged in research towards a Ph.D. at University College, London.

INTRODUCTION

The axially compressed circular cylindrical shell, although one of the simplest geometric forms, and under the action of such a simple axisymmetric load, displays a buckling phenomenon whose physical understanding and theoretical solution still present formidable obstacles. These obstacles, and the evident importance of cylindrical shell structures in the aircraft and space industries, and more recently in the marine platform industry, have led to considerable scientific effort being directed towards finding an explanation of its somewhat 'perplexing' behaviour. Many papers have been written covering both experimental and theoretical treatments, but it is probably still true to say that none can yet be considered to provide a satisfactory solution. Two excellent reviews of the subject are found in refs. [1, 2].

The discrepancies between the classical analytical predictions and the experimental values, and the scatter of these experimental results are enormous. Of the factors that have been advanced as possible reasons for both the discrepancies and scatter, the effect of initial imperfections has come to be accepted as the major cause. There seems to be general agreement in the literature [3–6] that end conditions (at least for practical situations) have a negligible influence on the experimental buckling load and behaviour of a circular cylindrical shell under axial compression. This has been substantiated by recent theoretical investigations [7, 8], which show that when the shell behaviour is dominated by the influence of initial imperfections, the effect of different boundary conditions (provided the circumferential and radial displacements are supressed) can be disregarded in the analysis.

Nevertheless, the studies that have been made on the effect of initial imperfections, although having achieved considerable success [7, 8], would seem to be unsuitable for incorporation into engineering practice. In reference [8] the relevant experimentally measured initial imperfection modes with amplitudes smaller than the shell's thickness were taken into account in a theoretical analysis, and good agreement between experimental buckling loads and the resulting critical loads were obtained. But application of this deterministic approach is currently limited by the lack of available imperfection data corresponding to various fabrication methods. Even when measurements of imperfection spectra of full scale structures are available, it is far from clear how the specifications of design tolerances, which may require consideration of the imperfection-sensitivity and control of many different possible combinations of imperfection

modes, will be made available to engineering practice. So that in the absence, in the literature, of simple and reliable theoretical estimates for the buckling load of axially compressed thin cylindrical shells, engineers to a large extent still rely on empirical formulae.

Due to the expected difficulty in controlling and measuring the initial imperfections and pre-buckling deformations while carrying out tests on full-scale structures, and also because of the difficulties of a subsequent analysis that takes into account gross initial imperfections and coupling between modes, alternative lines of research have been directed towards solutions that could provide lower bounds for the experimental results. Some attempts [9, 10] have been made in this direction by using advanced post-critical calculations to predict the minimum post-critical loads, and to use these as the lower limits for imperfection-sensitive buckling loads. But based on ref. [11] it has been argued [1] that these post-critical calculations are not as relevant as was at first thought. Not least of the problems associated with this method is the exceptionally difficult analysis, possibly requiring consideration of very many highly interactive modes, that is needed reliably to determine these post-critical minimum loads.

To overcome this practical obstacle an alternative approach has been proposed [12, 13], which attempts to define the physical characteristics in an advanced post-critical state so that they can be used as the basis of an equivalent eigenvalue analysis. The approach is based on the general notion that, for shells buckling into modes that derive their stability from the presence of significant membrane energy in the critical mode, any effect which undermines the membrane stiffness would give rise to substantial reductions in the buckling loads. These reductions in buckling loads would be due to the tendency for both imperfections and mode interactions to eliminate the membrane energy. In ref. [12] this approach was interpreted as simply setting the whole of the membrane strain energy in the critical modes equal to zero, which implies a quasi-inextensional solution of this problem. For the case of the axially loaded cylinder such a simplistic approach clearly could not account for many of the known behavioural characteristics.

The following, then, is an outline of a more systematic application of this general philosophy to the analysis of the axially loaded cylinder. The classical critical modes are first re-examined to isolate those components of the membrane stiffness most likely to be eroded in the non-linear buckling response. Based on this, a simplified analysis proposed in ref. [14] is developed and shown to compare favourably with the results of new and previously reported experimental evidence for this shell. Finally, it is

suggested how the simplified method could provide a safe and rational basis for future design of unstiffened cylinders under axial load.

CLASSICAL CRITICAL MODES RE-EXAMINED

The energy criterion requires that, for stability of a structural system to exist. the total potential energy, V, consisting of the sum of internal and external energy, shall be a minimum at the state of equilibrium. If the displacement components of the fundamental state (that is, the equilibrium configuration of the shell whose stability is to be investigated) are called, u^F, and the new configuration at some arbitrary neighbouring state, $u^F + u$, where u are kinematically admissible small incremental displacements, it follows that for stability

$$V(u^F + u) > V(u^F) \tag{1}$$

Using Taylor's expansion theorem, the left-hand side in eqn. (1) may be written as

$$V(u^F + u) \equiv V(u^F) + \delta V + \delta^2 V + \cdots \equiv V^F + V_1 + V_2 + \cdots \tag{2}$$

where, $V_1, V_2, \ldots$, are the first, second, ... variations of the total potential energy, that are linear, quadratic, ..., with respect to the incremental displacements, u, and their derivatives, and have coefficients that contain u^F as parameters.

In the following, the fundamental state of an axially compressed circular cylindrical shell is taken as a membrane state so that u^F is a linear function of the load parameter, λ, and the expansion (2) for the present loading case can be rewritten as [15, 16]

$$V[u^F(\lambda) + u] \equiv V[u^F(\lambda)] + V_1^o(u) + \lambda V_1'(u) + V_2^o(u) + \lambda V_2'(u) + V_3^o(u) + V_4^o(u) \tag{3}$$

where, the constant term $V[u^F(\lambda)]$ belongs to the fundamental membrane state. As the original configuration is a state of equilibrium,

$$V_1(u, \lambda) \equiv V_1^o(u) + \lambda V_1'(u) = 0 \tag{4}$$

which is satisfied by the membrane solution.

A necessary condition for stability is that the second variation of the total potential energy must be non-negative, requiring

$$V_2(u, \lambda) \equiv V_2^o(u) + \lambda V_2'(u) \geq 0 \tag{5}$$

The critical case of equilibrium occurs if $V_2(u, \lambda) \equiv 0$, for one or more linearly independent displacement fields, u. The condition of stationarity at the critical point,

$$\delta V_2(u, \lambda) = 0 \tag{6}$$

yields the eigenvalue problem whose solution gives the critical modes, $u = u^c$, and the critical load coefficients λ_c.

As the energy criterion for elastic stability is based on potential energy considerations, it will assist later discussion to observe how the different parts of the energy contribute to the second variation of the total potential energy about the critical point, $V_2(u^c, \lambda_c) \equiv 0$. Thus, breaking V_2 down into its constituent parts, this critical condition may be rewritten as

$$V_2 \equiv U_{2B} + U_{2M}^{x\theta} + V_{2M}^{x} + V_{2M}^{\theta} \equiv 0$$

or more completely

$$V_2 \equiv U_{2B}^{x} + U_{2B}^{\theta} + U_{2B}^{x\theta} + U_{2M}^{x\theta} + U_{2M}^{x} + \lambda_c V_{2M}'^{x} + U_{2M}^{\theta} + \lambda_c V_{2M}'^{\theta} \equiv 0 \tag{7}$$

where, U_{2B}^{x}, U_{2B}^{θ}, $U_{2B}^{x\theta}$, are respectively the axial, circumferential and twist bending strain energy contributions, U_{2M}^{x}, U_{2M}^{θ}, $U_{2M}^{x\theta}$ are the axial, circumferential and shear membrane strain energy contributions, and V_{2M}^{x}, V_{2M}^{θ} are the axial and circumferential membrane potential energies consisting of the two parts

$$V_{2M}^{x} = U_{2M}^{x} + \lambda_c V_{2M}'^{x}$$
$$V_{2M}^{\theta} = U_{2M}^{\theta} + \lambda_c V_{2M}'^{\theta}$$

In these membrane potential energies, $\lambda_c V_{2M}'^{x}$, $\lambda_c V_{2M}'^{\theta}$ are the axial and circumferential components of what is sometimes referred to as the load potential.

For the present loading case it is well known that the condition of stationarity (6) yields the classical eigenvalue problem, associated with the quadratic form in the identity (7), whose solution shows that many very close critical load coefficients, λ_c, occur for a family of critical modes, u_c. Investigation of the energy contributions for all these critical modes has been made in ref. [14], but for reasons of space only the most salient features of this analysis are presented here. In Fig. 1 the energy contributions for critical modes with one half axial wave ($j = 1$) are plotted as a function of the circumferential wave number, i. This shows that:

(a) the membrane energy is largely dominated by its axial membrane strain energy contribution, U_{2M}^{x}, with the circumferential membrane strain energy, U_{2M}^{θ}, negligible;

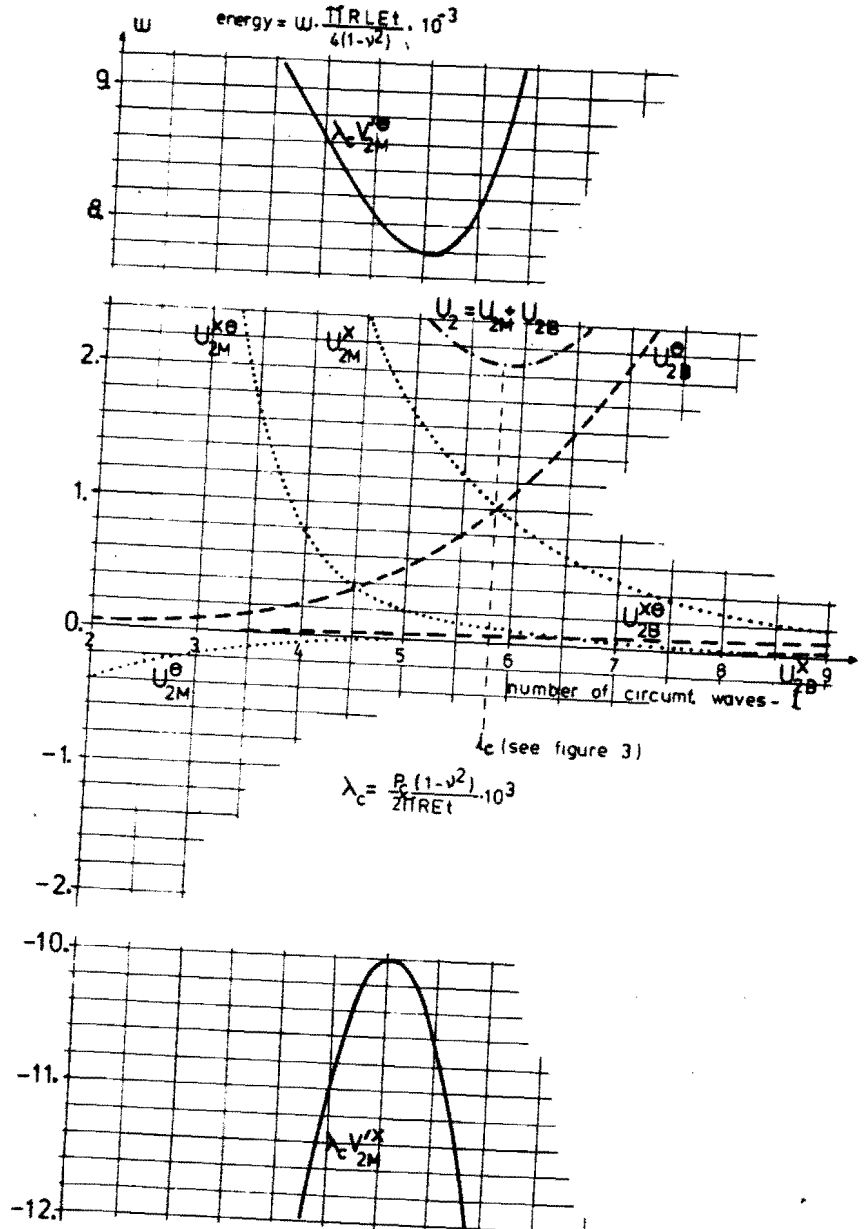

FIG. 1. Energy contributions to eqn. (7). $j = 1$ half axial wave; shell geometry, $L/R = 2{\cdot}88$, $R/t = 300$.

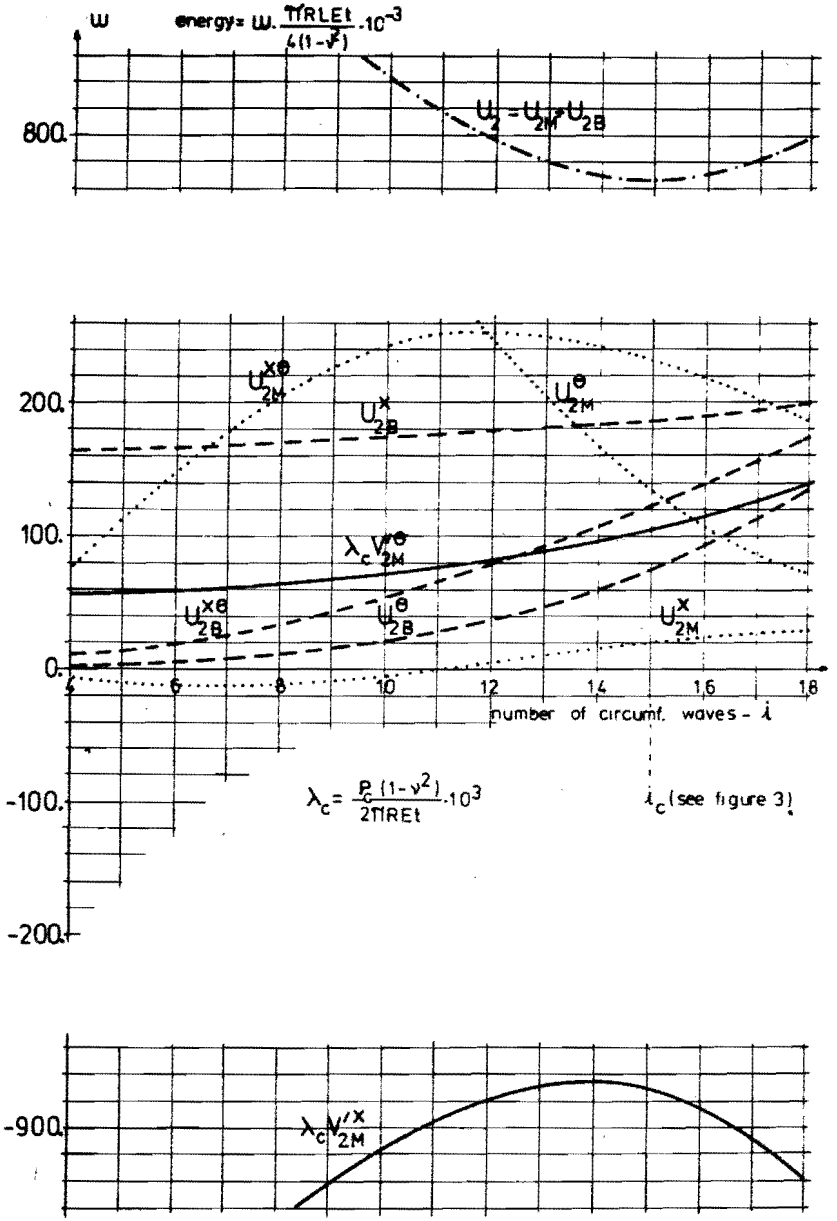

FIG. 2. Energy contributions to eqn. (7). $j = 20$ half axial waves; shell geometry, $L/R = 2{\cdot}88$, $R/t = 300$.

(b) the bending strain energy is largely made up of its circumferential component U^{θ}_{2B}, with the axial bending strain energy, U^{x}_{2B}, effectively zero;

(c) both the axial and circumferential load potential terms $\lambda_c V'^{x}_{2M}$ and $\lambda_c V'^{\theta}_{2M}$ have significant contributions to the second variation of the total potential energy, with the axial component destabilising, and the circumferential component stabilising the system.

In contrast, the energy contributions for modes with short axial wavelengths, of which the case of twenty half waves ($j = 20$) presented in Fig. 2 is typical, show that:

(a) it is now the axial membrane strain energy contribution that is almost negligible, with the membrane strain energy being dominated by its shear and circumferential contributions;

(b) all three bending strain energy terms have significant contributions to the bending energy, with its axial contribution dominating;

(c) compared with the one half axial wave, the total strain energy, $U_2 = U_{2M} + U_{2B}$, plays a relatively greater role than the circumferential load potential, $\lambda_c V'^{\theta}_{2M}$, in providing the resistance to instability.

PRESENT SIMPLIFIED APPROACH

It had been observed as early as 1934 [17] that an axially loaded cylinder, buckling into a mode with i circumferential waves and j half axial waves, will, as buckling progresses, tend to couple with axisymmetric components (consisting of a combination of a uniform radial contraction and the axisymmetric mode with $2j$ half axial waves) so as to relieve the shell of the need to develop circumferential membrane stresses. That is, a non-linear coupling can occur that will tend to reduce the effective circumferential membrane stiffness to zero. Figure 1 shows that this loss of circumferential membrane stiffness is likely to be particularly significant for the case of a single half axial wave. For it can be seen that in the $j = 1$ mode the major positive contribution to the second variation of the total potential energy, and therefore greatest stabilising influence, is that arising from the circumferential load potential term $\lambda_c V'^{\theta}_{2M}$, which is in turn directly related to the circumferential membrane stiffness of the shell. On the other hand, the circumferential membrane strain energy U^{θ}_{2M} is negligible. The net effect of a loss of circumferential membrane stiffness, however, would be a serious

destabilisation of the shell; and, because the axial bending strain energy associated with these long axial waves is negligible (at least for shells with $L/R > 0{\cdot}5$), this coupling and resultant loss of circumferential stiffness could be expected to occur with very little increase in the total bending energy. In contrast the relatively lower values of V^{θ}_{2M}, and the proportionally higher stabilisation provided by other components of the second variation of the total potential energy for short axial wavelengths, like that discussed in Fig. 2, suggest that the loss of circumferential membrane stiffness would be less significant for these short wavelengths. Furthermore, for short axial wavelengths j, the axisymmetric $2j$ mode with which it couples will also involve substantial additional axial bending strain energy. Simple physical reasoning combined with an analysis of the energy distributions in the classical critical modes, indicate that buckling will be accompanied by a loss of circumferential membrane stiffness, and that because this loss of stiffness has its most pronounced influence on the long axial wavelengths, it is these modes that could be expected to dominate the buckling process.

The importance of modes with long axial wavelength in the buckling behaviour of axially loaded shells had been suggested by Donnell and Wan [18] in the late nineteen-forties. More recently other workers [7, 8, 19] have reiterated the importance of these long axial waves through more refined buckling analyses in which full account is taken of small initial imperfections. In ref. [7] the sensitivity to long axial wavelength imperfection modes is demonstrated by an analysis of the combination of an asymmetric component (consisting of i circumferential waves and one half axial wave) with an axisymmetric component (consisting of a uniform axial contraction combined with the axisymmetric mode with 2 half axial waves). In this case, as already observed in ref. [17] the symmetrically deforming shell was shown to be relieved of the need to develop circumferential membrane stresses, resulting in a non-linearly de-stiffening response.

In contrast, there are no self-evident modes with which a critical mode having i circumferential waves and j half axial waves could couple so as to reduce to zero the incremental axial membrane stresses. Whereas the coupling to eliminate the incremental circumferential stresses could take place with the addition of little extra energy, especially for long axial wavelengths, the couplings required to annul the incremental axial membrane stresses would all involve substantial additional contributions of total energy and therefore stiffness.

It would appear therefore, that the combined effects of mode interactions

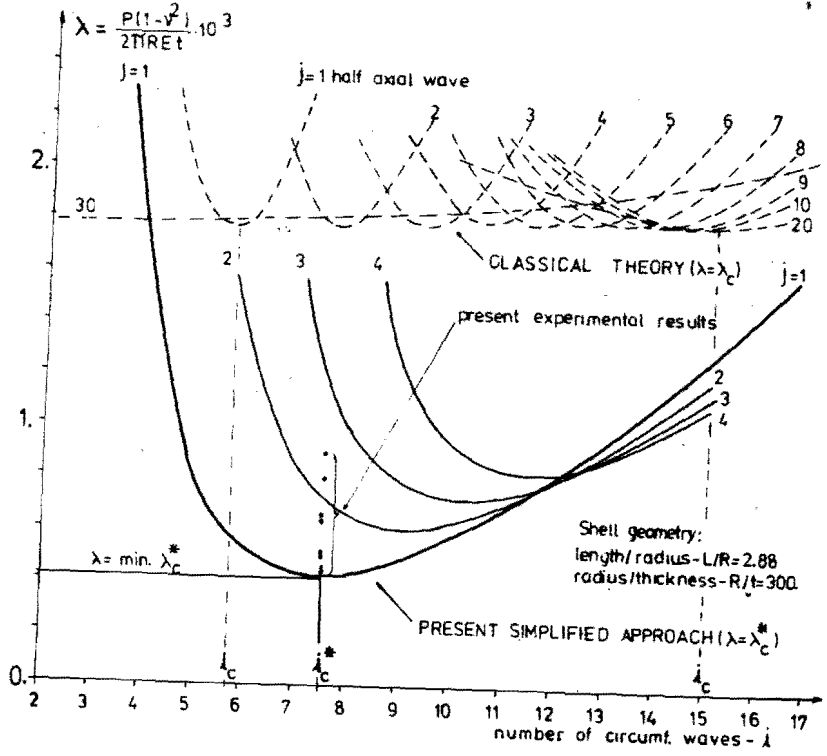

FIG. 3. Comparison between simplified and classical theories. Correlation with experiments.

and the de-stiffening caused by small initial imperfections, would result in only the circumferential membrane energy being lost during the buckling process. Assuming then, that the bending stiffness in a particular mode is not affected by small initial imperfections or mode coupling, and this is certainly the assumption conventionally made in non-linear analysis, a critical load analysis, in which the entire circumferential membrane energy is neglected, would from, eqn. (5), require

$$U_{2B} + U^{x}_{2M} + U^{x\theta}_{2M} + \lambda_c^* V'^{x}_{2M} \equiv 0 \qquad (8)$$

Now, the condition of stationarity (6) yields a reduced energy eigenvalue problem. The critical load coefficients λ_c^* obtained from this problem appear to be insensitive to end boundary conditions provided the out-of-plane deflection and the in-plane circumferential displacement are

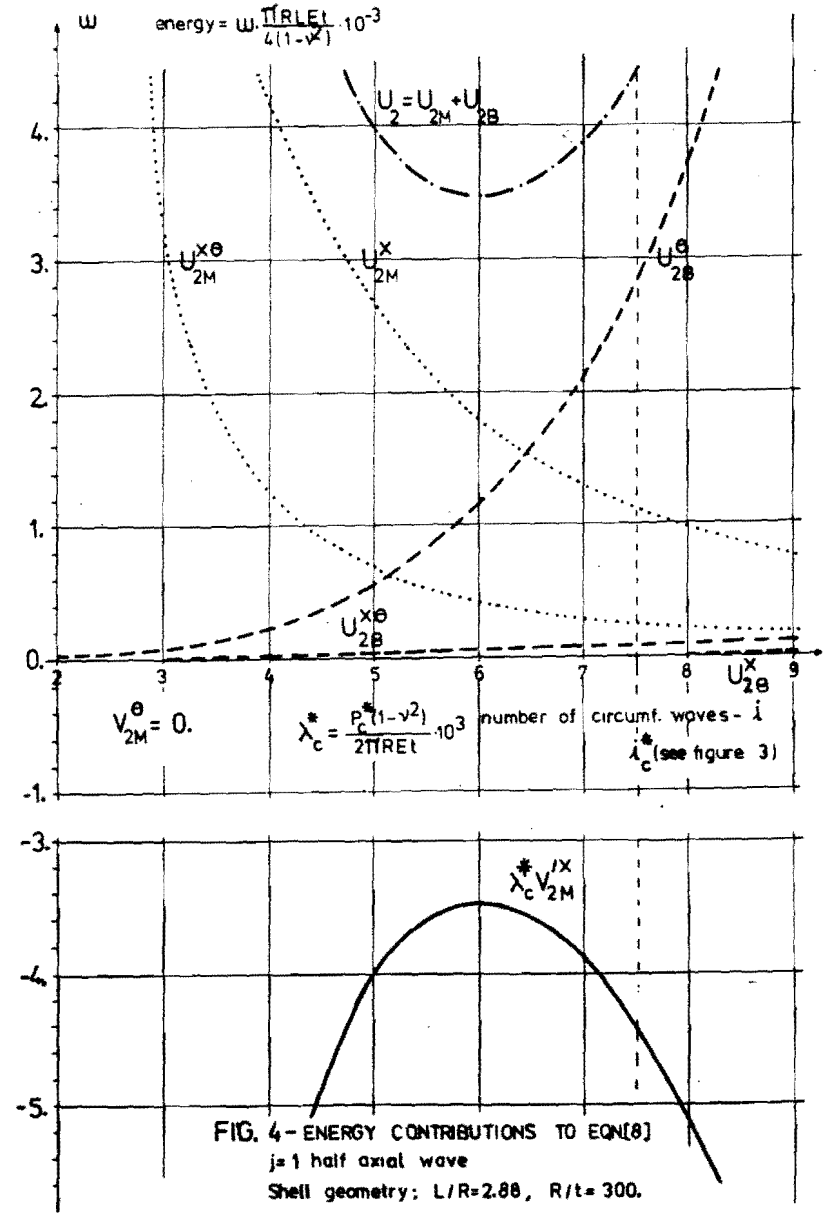

FIG. 4. Energy contributions to eqn. (8). $j = 1$ half axial wave; shell geometry, $L/R = 2{\cdot}88$, $R/t = 300$.

supressed [14]. The solution of this problem for simply supported ends has shown [14] that:

(a) unlike the classical theory, eqn. (7), the present simplified approach gives a well defined minimum critical load coefficient associated with a unique critical mode, this is shown in Fig. 3;

(b) this critical mode has only one half axial wave and a certain number of circumferential waves, i_c^*, which depends on the geometry of the shell. As in the case of the classical theory, for fixed values of R/t, i_c^* decreases with increasing L/R; for fixed values of L/R it increases with increasing value of R/t;

(c) the energy contributions, summarised for the $j = 1$ mode in Fig. 4, show that the bending strain energy is not affected by the assumed loss of circumferential membrane stiffness, but that some adjustment of the axial membrane energy has occurred;

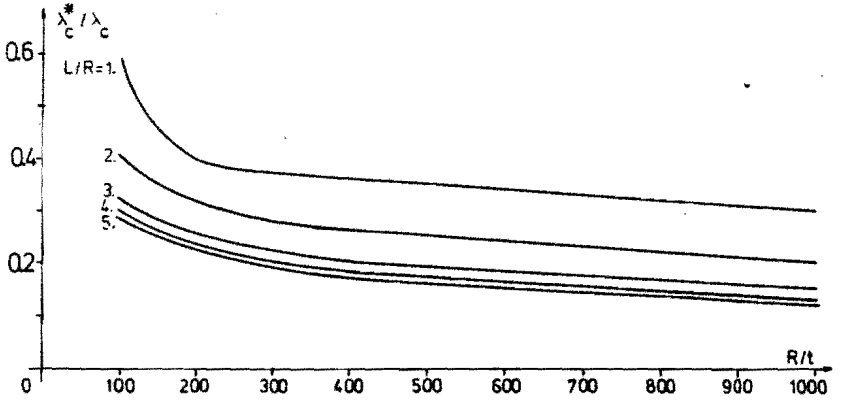

FIG. 5. Theoretical λ_c^*/λ_c curves for fixed L/R ratios.

(d) contrary to the prediction of the classical theory and to a well accepted idea by many investigators (perhaps due to the lack of concrete experimental evidence), the critical load as predicted by the present simplified approach, depends on the length of the shell even for values of $L/R \geq 1{\cdot}0$. The curves obtained from the present theoretical critical load coefficient over classical critical load coefficient ratios (λ_c^*/λ_c) with varying R/t ratio for different fixed L/R ratios are shown in Fig. 5, where for $L/R < 5$ the critical load predicted on the basis of the present theory is significantly affected by the precise value of L/R.

COMPARISON WITH EXPERIMENTS

To assess the accuracy of the present simplified theoretical approach in predicting the buckling wavelengths and the minimum experimental buckling loads as functions of the shell geometry, including the length effect, a number of experiments have been performed on commercially available thin-walled cylinders; these will be reported in greater detail elsewhere. In this experimental programme 46 steel and aluminium shells were tested and, for some of these shells, surface maps of the initial imperfections and the pre-buckling growth of radial displacements were obtained using a circumferential and axial traversing transducer, the output from which was plotted on an X–Y recorder. The main features observed during these experiments recover some of the findings reported in previous work by Arbocz and Babcock [4], and provide experimental confirmation of the analysis procedure outlined in the previous section. The experiments show that at the last load level prior to buckling, the shell models displayed a dominant mode with only one half axial wave covering the entire length of the shell, and that these one half axial wavelengths increased rapidly as the snap buckling load was approached. Along the circumferential direction these modes are characterised by a wavy shape with several relevant short wavelength components. Among these components the dominant one appeared to be strongly related to the shell's geometric parameters, length over radius (L/R) and radius over thickness (R/t), and was in accord with the i_c^* predicted on the basis of eqn. (8). The advanced post-buckled pattern, observed in all experiments, was characterised by the well-known diamond pattern in which the axial and circumferential wavelengths appear to be approximately the same.

Surface maps of the initial imperfections and pre-buckling radial displacements at a load close to the buckling load, P_b, for a typical shell model are shown in Figs. 6, 7(a) and 7(b). In Figs. 8 and 9 the corresponding circumferential harmonic contributions to the imperfection mode, and to the pre-buckling deformation mode at load levels around 90% of the eventual experimental buckling load, P_b, are analysed at mid-length of the shell. These figures show that the initial imperfection mode is dominated by long circumferential wavelengths, while the pre-buckling deformation mode is dominated by short circumferential wavelengths. Evidently then, the short wavelength components that dominated the circumferential pre-buckling deformation had relatively small values in the initial imperfection mode. What the harmonic analyses also show is the importance of the axisymmetric, $i = 0$, component in the pre-buckling deformation modes.

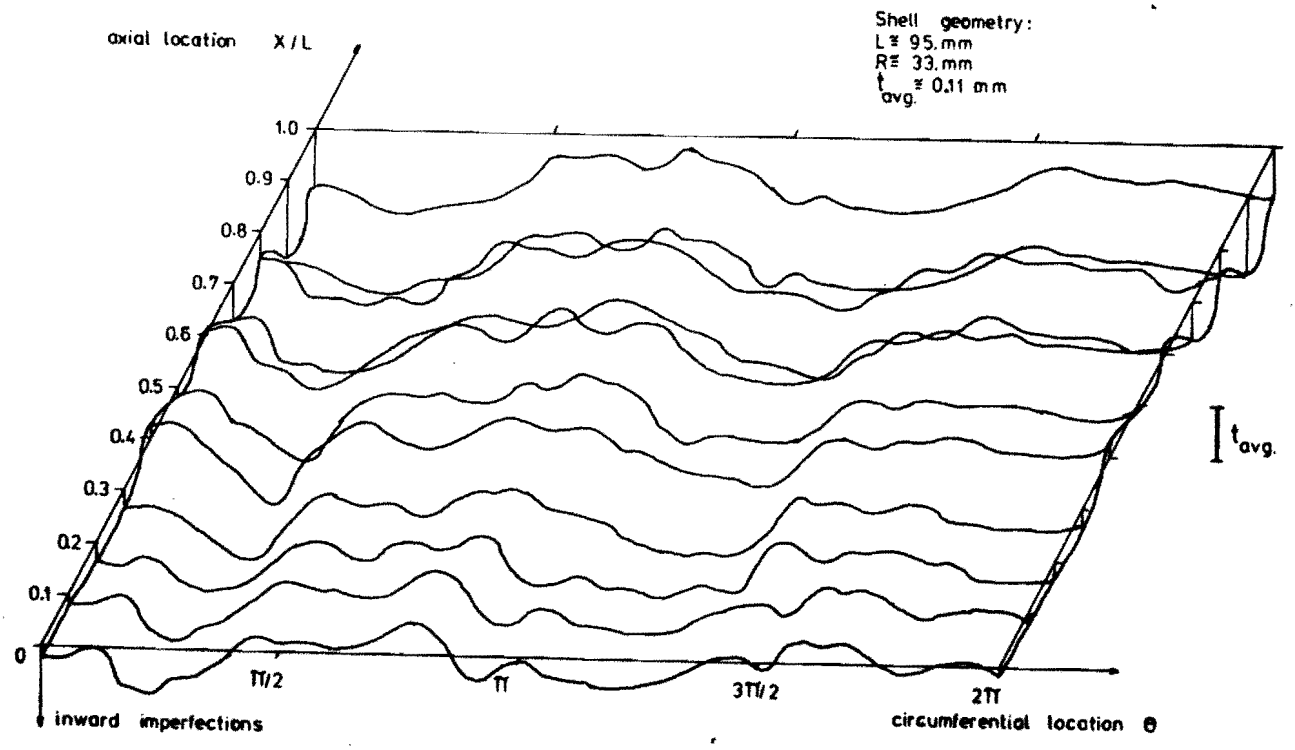

FIG. 6. Surface map of initial imperfections—circumferential profiles.

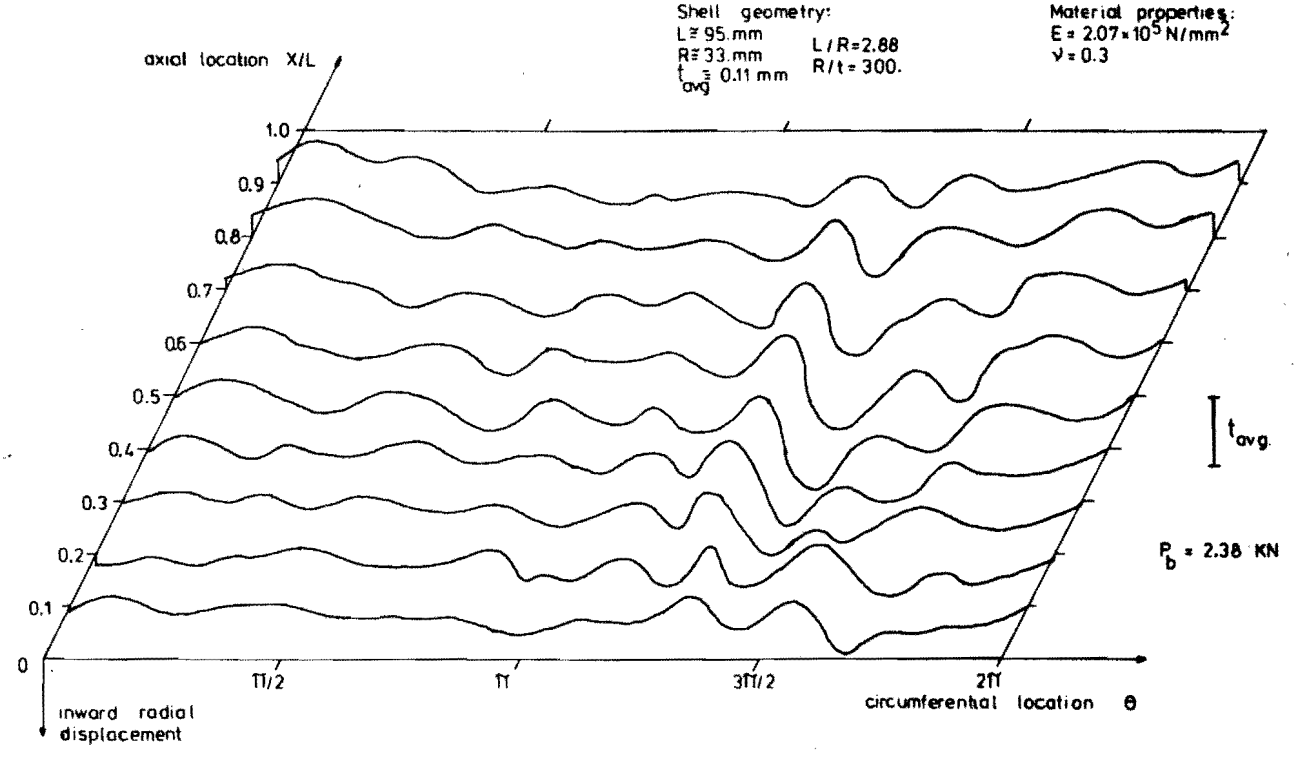

FIG. 7(a). Surface map of pre-buckling deformations at a load level equal to 0·87 × P_b—circumferential profiles.

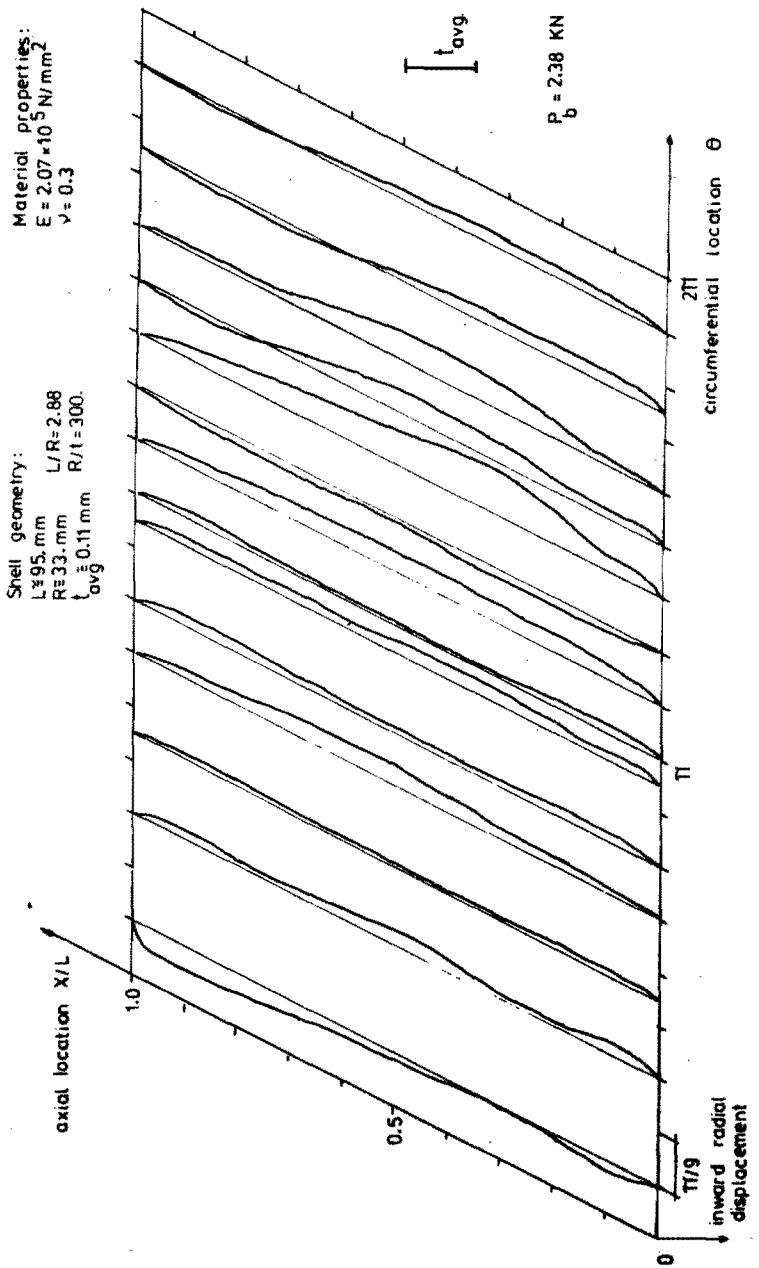

FIG. 7(b). Surface map of pre-buckling deformations at a load level equal to 0·87 × P_b—longitudinal profiles.

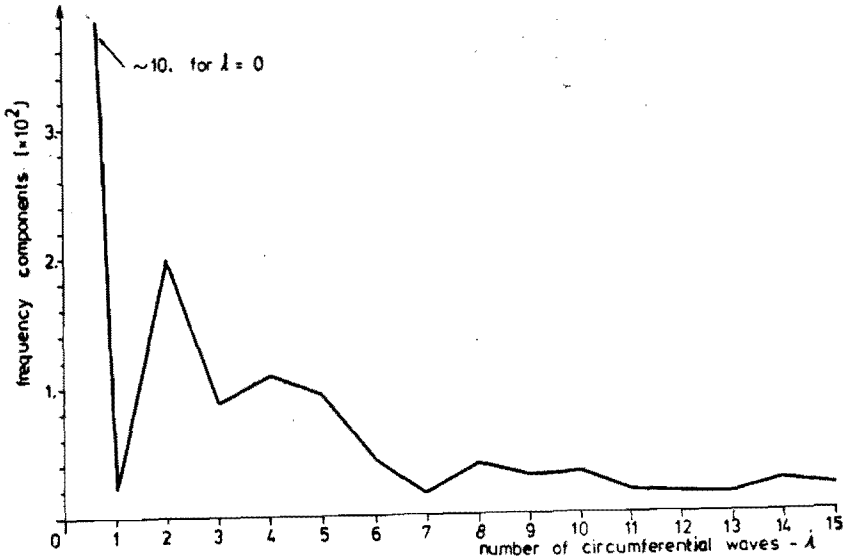

FIG. 8. Circumferential harmonic contribution to the imperfection mode at mid-length of the shell.

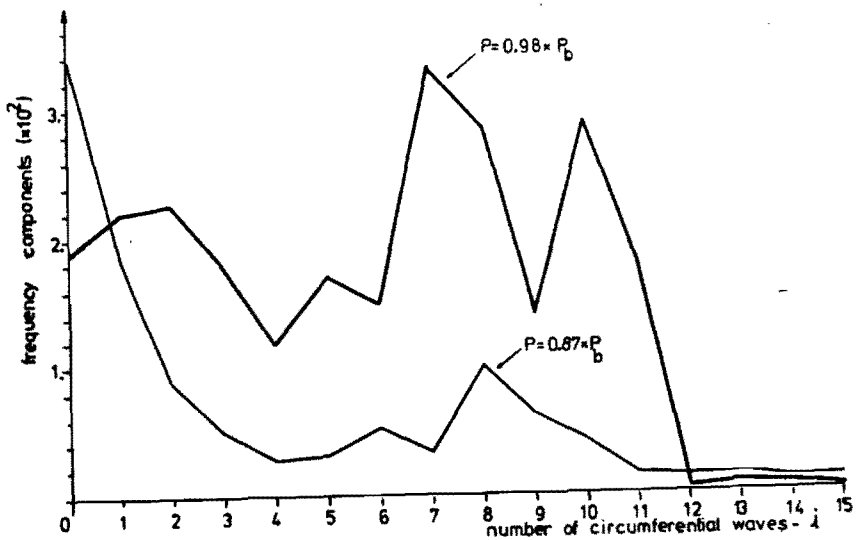

FIG. 9. Circumferential harmonic contribution to the pre-buckling deformation mode at mid-length of the shell.

These axisymmetric deformations, are of course, necessary to accommodate the low circumferential membrane stiffness assumed in the simplified analysis above.

In addition to the present experimental correlations, of which the above is merely typical, comparisons have also been made with over four hundred experimental results of axially compressed circular cylinders from over thirty references [2, 3, 20, 21, and those cited in these references]. Together with the results of the present experimental programme, these enable a number of general observations to be made. First, the critical number of full circumferential waves, i_c^* (or more precisely the critical wavelength) predicted by the simplified theoretical approach above is in close agreement with the dominant short wavelength mode components observed experimentally (this can be seen by comparing Figs. 3 and 9). Furthermore, the one half axial wave predicted by the present theory is also in agreement with the experimental observations as shown in Fig. 7(b). Unfortunately, the omission of information about the initial imperfections and the dominant mode components near or at buckling renders much of the existing experimental work of little value when it comes to the correlation between experimental buckling and theoretical critical modes. However, it is interesting to notice that a certain agreement is obtained when the circumferential critical modes predicted by the simplified approach are compared to the number of circumferential waves of the post-buckled dimple shape reported in some of the existing experimental works. This feature has been found to occur in the present experimental observations and is supported by past results [4], namely, that although the axial wavelength is changed, the dominant number of circumferential waves at the last load level prior to buckling is approximately the same as the number of circumferential waves in the post-buckled pattern.

The second general observation to emerge is that the critical load predicted by the present theoretical approach provides a lower bound to the imperfection-sensitive buckling loads. In Figs. 10(a)–10(c) the experimental buckling loads over classical critical load ratios (P_b/P_c) are plotted against their corresponding R/t ratios. These are selected collections of experimental data for shells with the L/R parameter within the fixed narrow ranges indicated on each of these figures. The curves obtained from the present theoretical critical load analysis, again normalised with respect to the classical critical load, are also plotted for the values of L/R related to the majority of the experiments. In these plots all reported experimental results from the above references were used, except, for obvious reasons, those from reference [41] in ref. [20], which belonged to a group of riveted

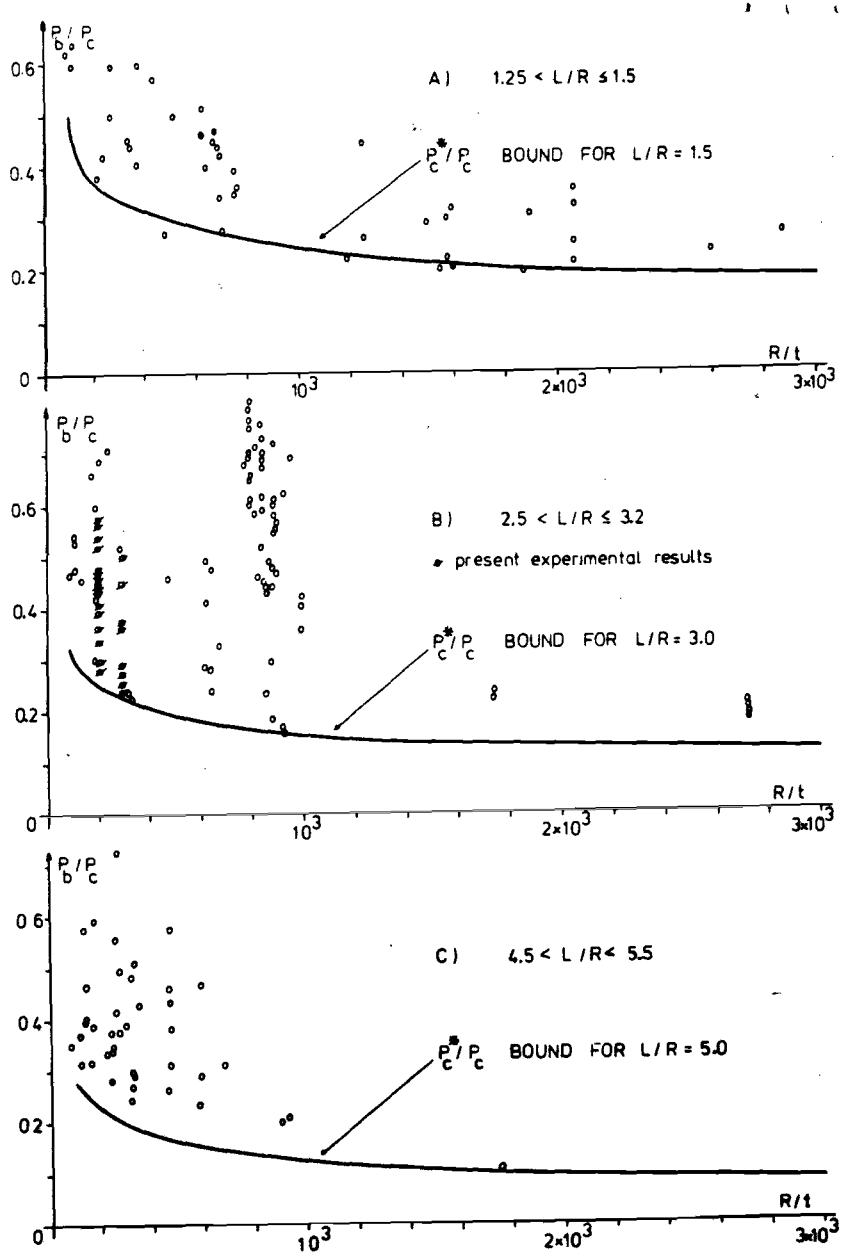

FIG. 10. Comparison between the present approach and collected experimental data for buckling of unstiffened cylinders within different L/R ranges.

models. Thus, to the extent that these collected data can be considered to represent a suitably wide sample of the experimental buckling loads, it appears that a slight dependence on the cylinder length does exist. Again, this confirms the prediction of the present theoretical approach. Although the length effect on the experimental buckling loads for short cylinders in which $L/R \leq 0{\cdot}5$ is well known [3] there is as yet little recognition of its importance for shells with $L/R > 0{\cdot}5$. But what these comparisons show most convincingly is the lower boundedness of the present theoretical predictions.

DESIGN APPROACHES

In the absence of reliable theoretical estimates for buckling of axially compressed cylinders, engineers have usually relied on empirical formulae [3, 22–24] which relate the buckling load coefficients to the single R/t parameter. Some of the design curves obtained from these formulae are shown in Fig. 11 together with that based on the theory of Donnell and Wan [18] which was proposed in ref. [20] as a lower bound for fabricated cylinders. The empirical curve proposed by Weingarten *et al.* [3] is a lower bound for selected test results from fourteen of the references given above, together with their own experimental results, and appears to be an accepted design criterion for isotropic aero-space shells. However, in the selection of the data, many buckling coefficients lower than their results were omitted on the premise that fabrication methods and testing techniques were significantly inferior; on this basis some of the classic experiments were therefore omitted. The other design curves shown in Fig. 11 have also been derived from empirical considerations and are intended for off-shore structures [22, 23] and pressure vessels [24]. In the same figure, the curves obtained from the present simplified critical load analysis are shown for values of L/R equal to 1·0 and 5·0. These represent approximately the smallest and largest L/R ratios for this vast collection of data.

The first thing to note is that depending on the value of L/R chosen the lower bound prediction from the present theoretical approach may be significantly affected. Secondly, that over a substantial range of R/t ratios the various past proposals for design lie somewhere between the lower bounds corresponding to the greatest and least value of L/R used in these tests. In taking what is therefore an effective average of the lower bounds for these different L/R ratios, past design proposals do not adequately allow for the rational inclusion of the L/R effect in design. For this reason they may

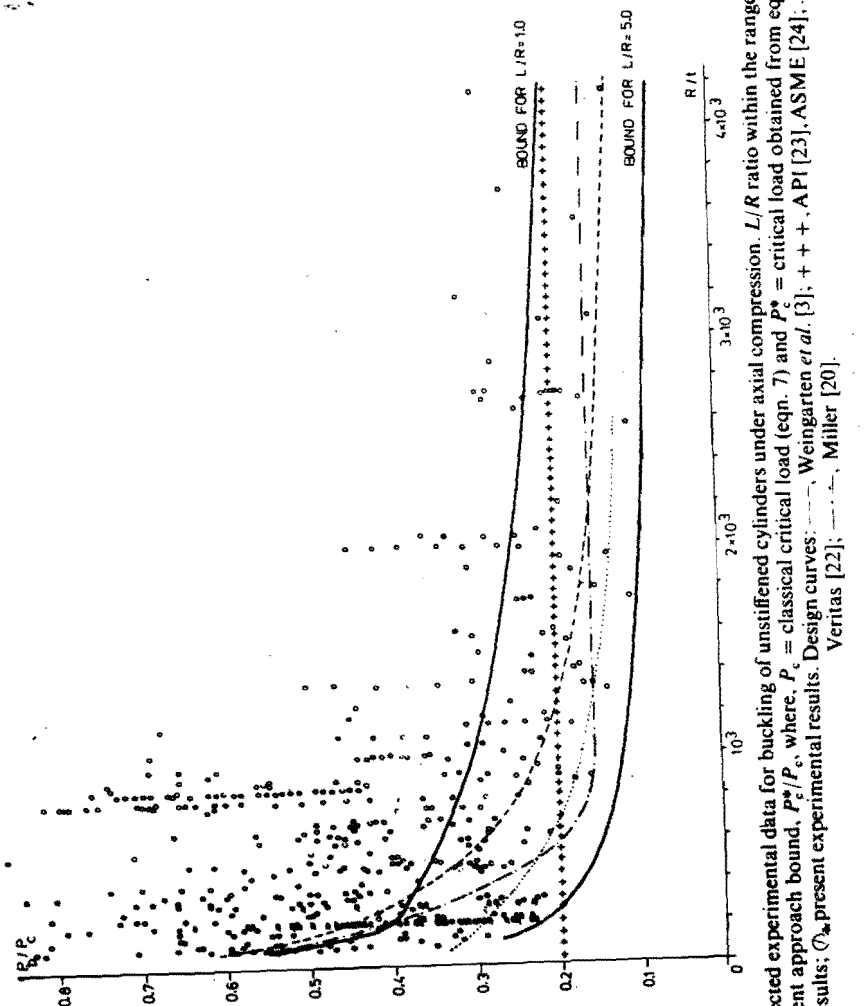

FIG. 11. Collected experimental data for buckling of unstiffened cylinders under axial compression. L/R ratio within the range, $0{\cdot}7 < L/R < 5{\cdot}5$. ——, Present approach bound, P_c^*/P_c, where, P_c = classical critical load (eqn. 7) and P_c^* = critical load obtained from eqn. (8); ○, past experimental results; ⊙, present experimental results. Design curves: — —, Weingarten *et al.* [3]; + + +, API [23], ASME [24]; · · ·, Det Norske Veritas [22]; — · —, Miller [20].

be over conservative for shells with small L/R ratios, but, more seriously, could provide non-conservative design loads if used for L/R ratios greater than those for which the design curves might be appropriate.

CONCLUDING REMARKS

The importance of the present simplified theoretical approach for buckling of circular cylindrical shells under axial compression is demonstrated by its simple and conservative estimation of buckling loads over a wide range of geometric parameters.

While the theories that seek to analyse the influence of gross initial imperfections in calculating the buckling loads present enormous difficulties, the present simplified approach provides reliable theoretical lower bounds of the buckling loads with a total effort comparable with that of the classical critical load analysis. But unlike the classical analysis the present approach successfully predicts the dominant buckling mode. Properly extended, the present simplified theoretical approach could eliminate the need for engineers to use 'knock down' factors or empirical formulae in designing cylindrical shells under axial compression.

ACKNOWLEDGEMENTS

The research reported in this paper was sponsored by CNPq (Brazilian National Council for Scientific and Technological Development) whose assistance is gratefully acknowledged.

REFERENCES

1. HUTCHINSON, J. W. and KOITER, W. T., Postbuckling theory. *Appl. Mech. Reviews*, **23,** 1970, 1353.
2. BABCOCK, C. D., Experiments in shell buckling, *Thin Shell Structures, Theory, Experiments and Design*, Part V, Eds Y. C. Fung and E. E. Sechler, Prentice-Hall, 1974, 345.
3. WEINGARTEN, V. I., MORGAN, E. J. and SEIDE, P., Elastic stability of thin-walled cylindrical and conical shells under axial compression, *AIAA Journal*, **3,** 1965, 500.
4. ARBOCZ, J. and BABCOCK, C. D., The effect of general imperfections on the buckling of cylindrical shells. *J. Appl. Mech.*, **36,** 1969, 28.
5. ALMROTH, B. O., Influence of edge conditions on the stability of axially compressed cylindrical shells. *NASA* CR-161, 1965.
6. HOFF, N. J. and SOONG, T. E., Buckling of circular cylindrical shells in axial compression. *S.U.D.A.E.R. No.* 204, Stanford, California, 1964.
7. ARBOCZ, J. and SECHLER, E. E., On the buckling of axially compressed imperfect cylindrical shells. *J. Appl. Mech.*, **41,** 1974, 737.
8. ARBOCZ, J. and BABCOCK, C. D., Prediction of buckling loads based on experimentally measured initial imperfections, *Proc. I.U.T.A.M. Symp. on Buckling of Structures, Harvard, Cambridge, Mass., June* 1974, Ed. B. Budiansky, Springer-Verlag, 1976.
9. VON KARMAN, T. and TSIEN, H. S., The buckling of thin cylindrical shells under axial compression. *J. Aero. Sci.*, **8,** 1941, 303.
10. ESSLINGER, M. and GEIGER, B., Calculated post buckling loads as lower limits for the buckling load of thin-walled circular cylinders, *Proc. I.U.T.A.M. Symp. on Buckling of Structures, Harvard, Cambridge, Mass., June* 1974, Ed. B. Budiansky, Springer-Verlag, 1976.
11. HOFF, N. J., MADSEN, W. A. and MAYERS, J., Post buckling equilibrium of axially compressed circular cylindrical shells. *AIAA Journal*, **4,** 1966, 126.
12. CROLL, J. G. A., Towards simple estimates of shell buckling loads, *Der Stahlbau*, **8,** 1975, 243.
13. CROLL, J. G. A., Coupled vibration mode. *J. Sound and Vibration*, **38,** 1975, 27.
14. BATISTA, R. C., Preliminary report on the buckling of circular cylindrical shells under axial compression, *Internal Report, Dept. of Civil & Municipal Eng.*, University College, London, 1977.
15. KOITER, W. T., *On the stability of elastic equilibrium*, Dissertation, Delft. Holland, 1945 (English trans. *NASA T.T.*, 1967).
16. THOMPSON, J. M. T. and HUNT, G. W., *A General Theory of Elastic Stability*. John Wiley and Sons, London, 1973.
17. DONNELL, L. H., A new theory for the buckling of thin cylinders under axial compression and bending. *Trans. ASME*, **56,** 1934, 795.
18. DONNELL, L. H. and WAN, C. C., Effect of imperfections on buckling of thin cylinders and columns under axial compression, *Trans. ASME, J. Appl. Mech.*, **17,** 1950, 73.
19. PEDERSEN, P. T., On the collapse load of cylindrical shells, *Proc. I.U.T.A.M. Symp. on Buckling of Structures, Harvard, Cambridge, Mass., June* 1974, Ed. B. Budiansky, Springer-Verlag, 1976.
20. MILLER, C. D., Buckling of axially compressed cylinders. *Proc. ASCE, J. Struct. Div.*, **103,** ST3, 1977, 695.
21. HARRIS, L. A., SUER, H. S., SKENE, W. T. and BENJAMIN, R. J., The stability of thin-walled unstiffened circular cylinders under axial compression, including the effects of internal pressure. *J. Aero. Sci.*, **24,** 1957, 587.
22. Det Norske Veritas, *Tentative rules for design, construction and inspection of fixed off-shore structures*, Rule proposal RMT-1-73, 1973.
23. American Pet. Inst., *Planning, designing and constructing fixed off-shore platforms*, API RP-2A Standard, Washington D.C., 1976.
24. *ASME, Boiler and pressure vessel code*. Section III Div. 1 (1974) and Section VIII Div. 1 and 2, addenda, Summer (1975).

for $\xi > 0$ and with $0 < \beta < 1$. For nearly all structures λ_1 is positive so that bifurcation takes place under increasing load, and λ_2 is negative. A similar expression with different constants λ_1, λ_2, β is valid for mode displacements in the opposite direction. The initial post-bifurcation behaviour predicted by the expansion (5) is illustrated in Fig. 2 for a symmetric and an asymmetric case. At asymmetric

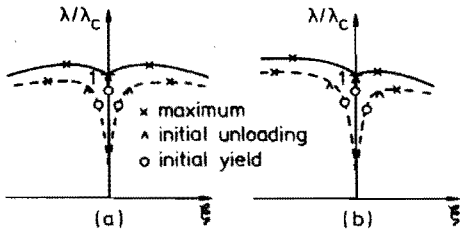

Fig. 2. Initial post-bifurcation behaviour in the plastic range in cases where the bifurcation mode is unique. Dashed curves show effect of small initial imperfections.

bifurcation the possibility remains that one of the two post-bifurcation paths does not initially involve elastic unloading, in which case the third term of (5) is replaced by a term of order $O(\xi^2)$ [32]. The extension of the asymptotic expansion (5) to cases of several coincident buckling modes has not yet been formulated.

While numerous investigations of bifurcation in the plastic range have been made, as referenced in a survey paper by Sewell [36], only relatively few investigations go beyond the bifurcation point. The various aspects of plastic post-buckling have been discussed thoroughly in Hutchinson's survey [33], and the asymptotic theory has been applied to study a few examples of structures with symmetric post-bifurcation behaviour [37,73] and asymmetric post-bifurcation behaviour [38,151,152] by Tvergaard and Needleman.

The effect of small initial imperfections on structures compressed into the plastic range has been discussed in detail by Hutchinson [39,33], but has not yet been described by a simple asymptotic formula such as Eqs. (2) and (3). One difficulty is that the maximum support load of the perfect structure is attained at a limit point after finite bifurcation mode deflections (Fig. 2) and not at the bifurcation point, as in the elastic range. Furthermore, an asymptotic expansion of the initial part of the equilibrium solution is only valid up to the point at which elastic unloading starts, while representation of the remaining part of the equilibrium path up to the maximum support load requires a second asymptotic expansion that accounts for the growing elastic unloading region [39].

For many structures with large destabilizing non-linearities the load at which unloading starts in the imperfect structure is only slightly below the maximum support load. In such cases a good indication of the imperfection-sensitivity is provided by an asymptotic estimate of this initial unloading load for a given imperfection [39,33]. In situations where bifurcation occurs in the elastic range, at stresses just below the yield stress, the load at which yielding first occurs for a given imperfection is sometimes representative of the imperfection-sensitivity [33].

For the special case of a cruciform column Hutchinson and Budiansky [40] have made an analytical investigation of imperfection-sensitivity in the plastic range, based on a hypoelastic theory (J_2 flow theory without elastic unloading). By using this hypoelastic theory the difficulties due to elastic unloading are avoided, and an asymptotic estimate of the imperfection-sensitivity is obtained in the form

$$\frac{\lambda_s}{\lambda_c} \approx 1 - \mu \bar{\xi}^{2/(2\Psi+1)} \qquad (6)$$

where $\mu > 0$ and $\Psi > 1$. The cruciform is exceptional in that, often, no strain rate reversal occurs before the maximum load, thus making Eq. (6) valid for elastic-plastic theory. A similar hypoelastic expansion has been used by Needleman and Tvergaard [41] to assess the imperfection-sensitivity of a square plate, for which unloading does occur before the maximum load. Even though this expansion does not account for unloading, the hypoelastic theory seems to reveal some of the main features of the elastic-plastic structure.

Bifurcation load predictions based on deformation theory are usually in better agreement with experiments than predictions based on the physically more acceptable flow theory of plasticity. As discussed by Hutchinson [33], this discrepancy may be explained by corners in the yield surface, or by a strong sensitivity to very small imperfections as in the extreme case of the cruciform column [40].

3. BUCKLING BEHAVIOUR OF THIN SHELLS

Among different types of structures the buckling behaviour of thin shell structures attracts special interest because of the many important applications and because some of these structures have an extremely unstable post-buckling behaviour, resulting in a very strong sensitivity to small initial imperfections. In this section a discussion is given of shell buckling behaviour based on investigations in the last few years, including investigations based on asymptotic post-buckling theory, purely numerical investigations, and experiments. A large number of earlier publications on the subject have been referenced by Hutchinson and Koiter [1], Brush and Almroth [3], and Babcock [42].

Cylindrical shells under axial compression. The long circular cylindrical shell under axial compression is probably the buckling problem

that has been paid most attention. In this case (Fig. 3a) bifurcation occurs at the classical buckling stress $\sigma_c = -\{3(1-\nu^2)\}^{-1/2} Eh/R$, but experiments show buckling loads that are only a small fraction of the classical load. This experimental scatter is very well explained by Koiter theory, as a result of interaction between several simultaneous buckling modes, so

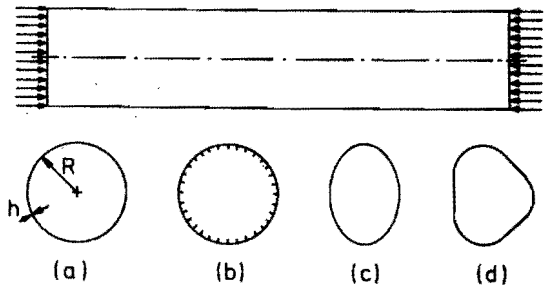

Fig. 3. Axially compressed cylindrical shells. (a) Isotropic shell. (b) Stringer-stiffened shell. (c) Oval shell. (d) Pear-shaped shell.

that, for example, an imperfection in the shape of the axisymmetric bifurcation mode with an amplitude of half the shell thickness reduces the buckling load to less than one-third of the classical [5]. The lowest order asymptotic predictions for more general imperfection shapes have recently been studied by Hansen [43], who finds that non-axisymmetric imperfections also reduce the load carrying capacity considerably, and that the behaviour due to any mixture of non-axisymmetric modes is described by only three imperfection parameters.

Instead of taking imperfections in the shape of the buckling modes, Arbocz and Babcock [44,45] have measured the imperfections of laboratory scale shells and have obtained quite good agreement between experimental buckling loads and buckling loads predicted by a multimode Galerkin solution of the nonlinear shell equations, or by an extended analysis [46] that also accounts for nonlinear prebuckling deformations due to edge constraints. Experimental investigations have also been reported recently in refs. [47,48]. It is well known that relaxing the in-plane boundary condition of zero tangential edge displacement may reduce the critical bifurcation load to about half the classical value [49]. However, Narasimhan and Hoff [50] have found that the imperfection-sensitivity corresponding to the reduced bifurcation load is far less than that obtained for classical simple support conditions.

For sinusoidal axisymmetric imperfections Koiter [51] has obtained an upper bound to the load at which the axisymmetric deformation bifurcates into an asymmetric shape (Fig. 4 for $k = \beta = \beta_c$) . Being based on a precise nonlinear prebuckling solution, this upper bound is valid even for rather large imperfections. It is therefore of interest to note that relatively small buckling loads are obtained compared with the experimental results, which are seldom below 25-30 per cent of the classical value, except for extremely thin shells. To explain this Budiansky and Hutchinson [52] have investigated the initial post-buckling behaviour at these bifurcation points, and they actually find a

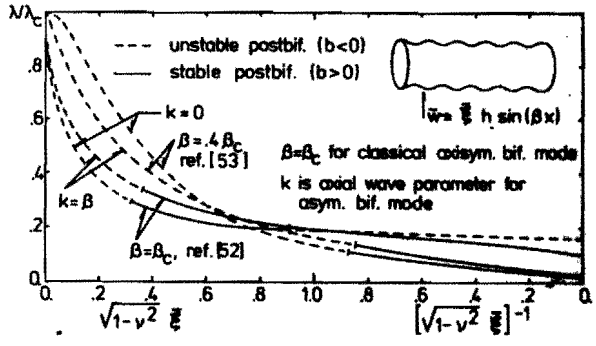

Fig. 4. Bifurcation loads based on nonlinear prebuckling analysis for axially compressed cylinder with sinusoidal axisymmetric imperfections.

transition from unstable to stable post-buckling behaviour as the bifurcation load drops below about 30 per cent of the classical value (Fig. 4 for $\beta = \beta_c$) . However, for imperfection wavelengths larger than that of the classical bifurcation mode, Pedersen [53] finds that this transition may take place at bifurcation loads below 15 per cent of the classical value (Fig. 4). In a subsequent paper Pedersen [54] has used a Galerkin solution to show that loads can be carried above the lower of these bifurcation loads, even though the initial post-bifurcation behaviour is unstable.

Closely ring-stiffened or stringer-stiffened circular cylindrical shells (Fig. 3b) are far less imperfection-sensitive than the isotropic shells. This is predicted by the asymptotic post-buckling analysis of Hutchinson and Amazigo [55], and a subsequent analysis [56] has shown that nonlinear prebuckling deformations due to load eccentricity or initial barreling may further reduce the imperfection-sensitivity. Bifurcation loads are clearly higher with stiffeners attached to the outside surface than with the same stiffeners attached to the inside surface, as was early observed by van der Neut [57], but, on the other hand, it turns out that outside-stiffened shells are more imperfection-sensitive.

Several experiments on stiffened shells machined out of aluminum or brass have been reported by Singer, Arbocz and Babcock [58], giving complete mappings of measured imperfections, and by Singer, Weller *et al.* [59-61], who take particular interest in edge effects such as load eccentricity. The experimental buckling loads obtained are in many tests as low as about 60